Inhibition of nonsense-mediated mRNA decay reduces the tumorigenicity of human fibrosarcoma cells

Sofia Nasif [1], **Martino Colombo** [1], **Anne-Christine Uldry** [2], **Markus S. Schröder** [3], **Simone de Brot** [4] **and Oliver Mühlemann** [1,*]

[1]Department of Chemistry, Biochemistry and Pharmaceutical Sciences, University of Bern, Switzerland, [2]Proteomics & Mass Spectrometry Core Facility, Department for BioMedical Research, University of Bern, Switzerland, [3]NCCR RNA & Disease Bioinformatics Support,Department of Biology, ETH Zürich, Switzerland and [4]COMPATH, Institute of Animal Pathology, University of Bern, Switzerland

ABSTRACT

Nonsense-mediated mRNA decay (NMD) is a eukaryotic RNA decay pathway with roles in cellular stress responses, differentiation, and viral defense. It functions in both quality control and post-transcriptional regulation of gene expression. NMD has also emerged as a modulator of cancer progression, although available evidence supports both a tumor suppressor and a pro-tumorigenic role, depending on the model. To further investigate the role of NMD in cancer, we knocked out the NMD factor SMG7 in the HT1080 human fibrosarcoma cell line, resulting in suppression of NMD function. We then compared the oncogenic properties of the parental cell line, the SMG7-knockout, and a rescue cell line in which we re-introduced both isoforms of SMG7. We also tested the effect of a drug inhibiting the NMD factor SMG1 to distinguish NMD-dependent effects from putative NMD-independent functions of SMG7. Using cell-based assays and a mouse xenograft tumor model, we showed that suppression of NMD function severely compromises the oncogenic phenotype. Molecular pathway analysis revealed that NMD suppression strongly reduces matrix metalloprotease 9 (MMP9) expression and that MMP9 re-expression partially rescues the oncogenic phenotype. Since MMP9 promotes cancer cell migration and invasion, metastasis and angiogenesis, its downregulation may contribute to the reduced tumorigenicity of NMD-suppressed cells. Collectively, our results highlight the potential value of NMD inhibition as a therapeutic approach.

GRAPHICAL ABSTRACT
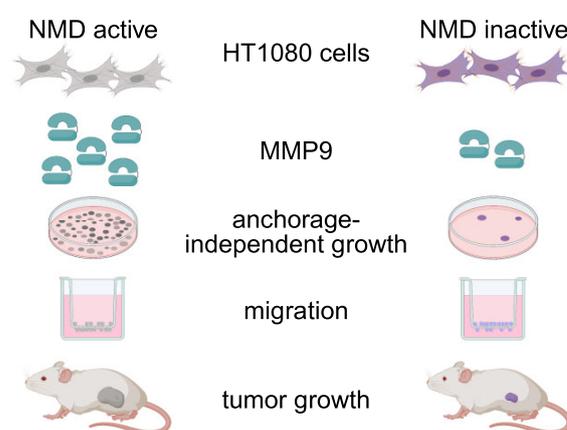
INTRODUCTION

Fidelity of gene expression is essential for every living organism, which is why prokaryotic and eukaryotic cells put into play a myriad of quality control pathways to ensure that faulty RNAs and proteins are recognized and degraded. Of particular importance are RNA surveillance pathways, which not only degrade faulty RNAs but also control the levels of RNA molecules and thereby contribute to post-transcriptional gene regulation (1). In eukaryotes, the separation of transcription and translation in different cellular compartments allows for the compartmentalization and functional distinction between decay pathways aimed at degrading aberrantly processed RNAs and transcriptional by-products, which are mainly nuclear, and decay pathways aimed at identifying and degrading RNAs with hampered functionality, most of which are cytoplasmic (2). One such cytoplasmic mRNA decay pathway is nonsense-mediated mRNA decay (NMD), which was first

*To whom correspondence should be addressed. Tel: +41 31 684 46 27; Email: oliver.muehlemann@unibe.ch

described as a translation-dependent mechanism responsible for the rapid decay of mRNA molecules harboring premature termination codons (PTC) (3–5). PTC-bearing mRNAs arise in eukaryotic cells as results of DNA mutations and errors occurring during transcription or splicing. In this context, NMD serves as a safeguard mechanism to prevent the production of truncated proteins that can have deleterious effects on cells. More recently, genome-wide studies revealed a much larger influence of NMD on the transcriptome of eukaryotic cells (6–11), with the latest estimates suggesting that NMD activity can modulate – directly and indirectly – the abundance of up to ∼40% of the transcriptome in human cells (12). These studies showed that NMD can also target for degradation mRNAs encoding functional full-length proteins and expanded the perception of NMD as a quality control pathway that can, additionally, exert fine post-transcriptional control of gene expression.

The mechanism of mammalian NMD has been studied in detail (reviewed in (13)). It relies on several proteins that work sequentially, and jointly, to decide the fate of the mRNA molecules. The core NMD factor is UPF1 (Up-frameshift 1), an ATP-dependent helicase that binds all mRNAs without sequence specificity (14). Selection of substrate mRNAs relies on the completion of two steps: first, activation of UPF1 by phosphorylation, mediated by the kinase SMG1 (Suppressor with morphogenetic effects on genitalia 1) and facilitated by the UPF1 interaction partners UPF2 and UPF3B, and second, recruitment of the decay effector proteins SMG5, SMG6 and SMG7 that trigger the degradation of the mRNA (13). SMG6 is an endonuclease that cleaves the mRNA in the vicinity of the stop codon (15), while SMG5 and SMG7 form a heterodimer that triggers the exonucleolytic decay of the transcript by recruiting the CCR4-NOT complex (16). There is a big overlap in the mRNAs that are targeted by the three effector proteins, suggesting that they operate with some level of redundancy (10–12,17). In addition, it has been recently reported that the SMG5 and SMG7 proteins play a role in enabling SMG6-mediated endonucleolytic cleavage (12), indicating that the three NMD effector proteins work together, rather than in parallel, to trigger mRNA decay. A full understanding of the mechanistic aspects of mammalian NMD is further obstructed by its autoregulation, i.e. most of the mRNAs encoding NMD factors are substrates of the NMD pathway, and are therefore upregulated when NMD activity is compromised, attempting to restore NMD (9,18). Additionally, it has recently been reported that NMD inhibition also results in a feedback loop, mediated by the accumulation of the NMD sensitive EIF4A2 mRNA, that boosts translation initiation. Since NMD is a translation-dependent mechanism, this feedback loop is also interpreted as trying to recover NMD activity (17). The existence of such regulatory feedback loops suggests that NMD is indispensable for cellular fitness, a notion further supported by the fact that depletion of NMD factors results in reduced viability (reviewed in (19)).

Since nonsense and frameshifting mutations account for approximately 30% of all disease-associated genetic variants, NMD's capacity of detecting and degrading PTC-containing mRNAs makes it an important modulator of the outcome of genetic diseases (20). NMD can have oppos-

ing roles in modulating disease severity; it can be beneficial in cases where the expression of truncated proteins would have dominant negative effects, or it can worsen the disease phenotype in cases where the truncated protein would still retain some activity (20). One disease that is highly dependent on the accumulation of genetic mutations is cancer, and the link between NMD activity and cancer progression is a topic of intensive research (reviewed in (21)). There is abundant evidence supporting a pro-tumorigenic role for NMD. For instance, it has been shown that depletion of the NMD factors UPF2, UPF1 or SMG1 results in reduced *in vivo* tumor growth in a variety of cancer types, due to the strong anti-tumor immune response elicited by the NMD-deficient tumors (22–25). mRNAs containing frameshifting mutations can be translated into novel peptides, that can be recognized as foreign by the immune system and trigger an immune response. By degrading these mutant transcripts, NMD reduces the expression of neoantigens and therefore helps the tumor evade the immune attack (22–28). Further evidence that tumors benefit from high NMD activity comes from pan-cancer genome-wide mutational studies that discovered that tumor suppressor genes preferentially accumulate NMD-eliciting nonsense mutations, while oncogenes are depleted of NMD-inducing mutations (29,30). Additionally, it has been reported that the genes encoding core NMD factors are amplified in multiple types of cancers and that this is associated with higher NMD efficiency and lower cytolytic activity (31). Moreover, it was recently shown that in tumors undergoing immunotherapy, the immunosuppressive IL-6/STAT3 signaling pathway induces SMG1 levels, and NMD activity, to suppress the expression of potent frameshift-derived neoantigens (24). Another way in which NMD can promote cancer is by degrading mRNAs encoding for truncated, though still functional, tumor suppressor proteins (32–35). On the other hand, there is also evidence supporting a role for NMD as a tumor suppressor pathway. For example, it has been reported that UPF1 levels are decreased in tumor tissue, relative to normal adjacent tissue, in different cancer types (36–40). Also, a functional interplay between the tumor microenvironment and NMD has been suggested, by which cellular stressors like starvation and hypoxia reduce NMD activity and this, in turn, promotes tumorigenesis (38,41).

To gain more insight into the molecular underpinnings of the links between NMD activity and cancer progression in a well-established tumor model, we decided to study the role of the NMD factor SMG7 in the tumorigenicity of the human fibrosarcoma cell line HT1080. We generated SMG7 knockout (KO) HT1080 cells and confirmed that they have impaired NMD. Using *in vitro* cell-based assays as well as mouse xenografts, we found that NMD-inhibited HT1080 cells display impaired tumorigenicity. Gene expression analysis revealed that NMD inhibition resulted in a greatly reduced expression of the pro-tumorigenic gene MMP9, and that the impaired tumorigenicity of the SMG7KO cells can be partially rescued by MMP9 overexpression. Our results show that in this fibrosarcoma model, NMD activity is beneficial for tumor progression and suggest that NMD inhibition would represent a promising therapeutic approach for this type of tumors.

MATERIALS AND METHODS

Cell lines and cell culture

HT1080 cells (CCL-121™, ATCC®), and all cell lines derived from them, were cultured in Dulbecco's modified Eagle's medium (DMEM) supplemented with 10% fetal calf serum (FCS), 100 U/ml penicillin and 100 μg/ml streptomycin (P/S) at 37°C under 5% CO_2. TNFα treatment (25 ng/ml rh TNF-alpha, STEMCELL Technologies) was performed in DMEM without FCS for 20 h, unless otherwise stated. NMD inhibition (NMDi) was achieved by supplementing the medium with 0.3 μM of a SMG1 inhibitor (hSMG1-inhibitor 11e, PC-35788 ProbeChem®). When NMDi and TNFα treatments were combined, cells were first treated for 24 h with NMDi and then TNFα was added for 20 h before harvesting. For the mRNA stability measurements, HT1080 cells in 6-well plates were first treated with TNFα (25 ng/ml) for 24 h, in the presence of DMSO or NMDi 0.3 μM. Next day, Actinomycin D (ActD 1 μg/ml) was added to all wells, without exchanging the growth medium. Cells were harvested 0, 5, 8, 15 and 24 h after ActD addition and RNA extraction and RT-qPCR were performed as described below.

SMG7KO cells were generated by introducing a gene trap into the first intron of the SMG7 gene, via CRISPR-Cas9 genome editing, as described in (42). Single cell-derived clones were picked after Zeocin selection and two of them, SMG7KO_11 and SMG7KO_12, were used here.

The RESCUE cell line was generated by re-introducing both isoforms of SMG7 in the SMG7KO_12 clone, using the AAVS1 Safe Harbor Targeting System (GE622A-1-SBI, System Biosciences). In the first round of genome editing, a construct encoding the N-terminally 3xFlag-tagged short isoform of SMG7 (3xFlag-SMG7short) and a puromycin resistance gene was used. After transfection, cells were selected for 10 days with puromycin (2 μg/ml) and single cell-derived clones were picked. The clones were analyzed by screening for SMG7 mRNA expression using qPCR, and expression of 3xFlag-SMG7short was confirmed by western blotting (WB). Next, a clone expressing 3xFlag-SMG7short was subjected to a new round of genome editing, in which we introduced a N-terminally HA-tagged SMG7long expression cassette along with a blasticidin resistance gene. After selection for 10 days with 6 μg/ml blasticidin, single cell-derived clones were picked and analyzed by WB to confirm the expression of both SMG7 isoforms.

To generate the MMP9 overexpressing (MMP9OE) cell line, the MMP9 coding sequence was amplified from cDNA of one of the tumors formed by HT1080 cells (Tumor WT_674) and subcloned into a pcDNA5-derived expression vector, in which the hygromycin resistance gene was replaced by a PGK promoter followed by a puromycin selection cassette. Subcloning into this vector also introduced a 3xFlag tag in the C-terminus of MMP9. This plasmid was then used to generate a cell line that constitutively expresses MMP9-3xFlag. For this, SMG7KO_12 cells were transfected with the expression plasmid and selected for 10 days with 1 μg/ml puromycin. Stably transfected cells were kept as a pool, and MMP9 expression and gelatinolytic activity was confirmed by performing WB with anti-

MMP9 and anti-Flag antibodies and gelatin zymography, respectively.

Cellular transfection

Plasmid transfections to generate stable cell lines were performed with TransIT®-LT1 transfection reagent (Mirus). 2×10^5 cells per well were seeded in 6-well plates the day before transfection, transfection complexes containing 3 μl of the transfection reagent per μg of transfected DNA were prepared in Opti-MEM™ (Gibco) medium, incubated 20 min at room temperature and then added onto the cells. The medium was exchanged on the following day and antibiotic selection started on the third day after transfection.

For siRNA transfections, 2×10^5 cells per well were seeded into a 6-well plate and transfections were performed using the Lullaby transfection reagent (OZ Biosciences). Transfection complexes were prepared in Opti-MEM™ (Gibco) medium and consisted of 5.6 μl of the transfection reagent and 22 nM siRNA in a final volume 2 ml/well. Cells were transfected twice with the siRNAs, on the first and third days after seeding, and harvested one day after the second transfection.

Protein analysis by western blotting

Cellular protein levels were analyzed by lysing cells in RIPA buffer (10 μl per 1×10^5 cells; 10 mM Tris–HCl pH 8.0, 1 mM EDTA, 1% Triton X-100, 0.5% sodium deoxycholate, 0.1% SDS, 150 mM NaCl, supplemented with protease and phosphatase inhibitors), followed by WB. Typically, lysate corresponding to 2×10^5 cell equivalents was mixed with loading buffer (NuPAGE™ LDS Sample Buffer, Thermo Fisher Scientific) containing 50 mM DTT, heated for 10 min at 70°C, and loaded onto NuPAGE™ 4–12% Bis–Tris gels (Thermo Fisher Scientific). Transfer to nitrocellulose membranes (iBlot™2 Transfer Stacks, Thermo Fisher Scientific) was done with the iBlot2 Dry Blotting System (Thermo Fisher Scientific), using the P0 standard program. After blocking for 1 h at room temperature with 5% BSA (in 20 mM Tris, 150 mM NaCl, 0.1% (v/v) Tween 20, pH 7.4), membranes were probed with the specified primary antibodies (diluted in blocking solution), either for 2 h at room temperature or overnight at 4°C. We used fluorophore-coupled secondary antibodies and fluorescent signals were detected using the Odyssey Infrared Imaging System (LI-COR Biosciences). The antibodies used in this study are listed in Supplementary table S4.

For studying the levels of secreted proteins, 2 ml of conditioned media were collected from nearly confluent 6-well plates, centrifuged for 10 min at 16 000 g and the cleared supernatant was transferred to a new tube. Half of the collected material was stored at –80°C, while the other half was subjected to protein precipitation with acetone. Precipitated proteins were resuspended directly in loading buffer (NuPAGE™ LDS Sample Buffer, Thermo Fisher Scientific) and loaded onto NuPAGE™ 4–12% Bis–Tris gels (Thermo Fisher Scientific). After proteins were transferred to nitrocellulose membranes, they were stained with Revert700 total protein stain (LI-COR

Biosciences) and imaged using the Odyssey Infrared Imaging System (LI-COR Biosciences), for normalization. After the total protein stain was removed, the WB protocol was followed as described above. Densitometric quantification of the western blots was done using ImageJ software.

RNA extraction and mRNA expression analysis by RT-qPCR

Total RNA from cultured cells was isolated using the guanidium thiocyanate–phenol–chloroform extraction protocol followed by isopropanol precipitation as described in (43). Residual DNA was removed with the TURBO DNA-free™ kit (Thermo Fisher Scientific) and RNA concentration was measured by NanoDrop 2000 spectrophotometer (Thermo Fisher Scientific). Next, 1 μg of RNA was reverse transcribed using random hexamers and the AffinityScript Multi-Temp reverse transcriptase (Agilent) following the manufacturer's instructions. cDNA levels were measured by quantitative real-time PCR using Brilliant III Ultra-Fast SYBR Green qPCR mix (Agilent) and 24 ng of cDNA, in 15 μl reactions. For detection of pre-mRNAs by RT-qPCR 75 ng of cDNA were used in 15 μl reactions. Cycling and fluorescence acquisition were done with the Rotor-Gene Q (Qiagen). RT minus reactions were run in every experiment to control for DNA contamination, when measuring pre-mRNA levels, RT minus reactions were run for every sample, in every experiment. All the assays used in this study have an amplification efficiency of 1, allowing the use of the $\Delta\Delta$Ct method for relative quantitation. The primer sequences used for qPCR can be found in Supplementary Table S4.

To extract total RNA from the tumor samples, the tissue was first lysed and homogenized by dual centrifugation at 2500 rpm, –5°C for 4 min using the ZentriMix 380R (Hettich) and RNA was purified using the GeneElute™ Mammalian Total RNA Midiprep Kit (Sigma Aldrich) following the manufacturer's instructions, including the in-column DNAse digestion step. The extracted RNA was then reverse transcribed and cDNAs were quantified by qPCR as described above. For measuring SMG7 expression levels in the tumor samples, a SMG7 TaqMan qPCR assay was used, because it is specific for detecting SMG7 of human origin. For this, the Brilliant III Ultra-Fast qPCR mix (Agilent) was used.

RNAseq analysis

The RNAseq analysis of the HT1080, SMG7KO_11 and SMG7KO_12 cell lines were first described in (42). Libraries were prepared with the Illumina TruSeq Stranded Total RNA Library Prep Kit (chemistry v3), including a ribo-zero depletion step. The reads (100 base pairs and in single-end mode) were produced by means of a HiSeq3000 machine, reaching a sequencing depth of around 85 million per sample. Every condition was analyzed in triplicate. Read mapping was performed with STAR 2.7.8a to the full human genome, version GRCh38.10.9, without providing a reference annotation. Read counting was carried out with featureCounts (Subread package) version 2.0.1 on Ensembl GRCh38 release 109. The chosen options were: reverse strand (-s 2), multi-mapping allowed (-M), fractional

assignment (–fraction). The differential analysis was performed with DESeq2, version 1.40.0. Technical replicates sequenced on different lanes were merged, while biological replicates showed very high consistency. The two clones were analyzed separately and compared to the parental line. A meta-analysis of the two analyses was computed with the sum of *P*-value method.

For the transcriptomic analysis of the tumor samples, libraries were prepared with the Illumina TruSeq Stranded Total RNA library kit, including rRNA depletion. The NovaSeq6000 instrument was used to produce 50 bp paired-end reads, obtaining on average 25 million reads per sample. Three independently grown tumors from HT1080 cells and two independently grown tumors from SMG7KO and RESCUE cells were analyzed. Reads were mapped to a combined version of GRCh38.p12 (GenBank assembly accession: GCA_000001405.15) and mm10 (ENCODE dataset: ENCSR425FOI) using STAR version 2.7.2b with options 'runThreadN 40' and 'twopassMode Basic'. Read counts were generated with featureCounts version 1.6.4 with option '-p -T 50 -t exon -g gene_id', using a merged annotation of Ensembl GRCh38 version 97 and mm10 GENCODE_VM21 (ENCODE dataset: ENCSR425FOI). DESeq2 version 1.24.0 was used to identify differentially expressed genes.

All differential gene expression analyses reported in this manuscript are gene-level analyses.

Proteomic analysis by SILAC and MS/MS

HT1080, SMG7KO_11 and SMG7KO_12 cells were grown for 8-cell doublings in SILAC labelling medium (44). Each cell line was labelled once with light- and once with heavy-amino acids. After harvesting, cells were lysed in lysis buffer (8 M urea in 100 mM Tris–HCl pH 8.0) supplemented with protease inhibitors. Next, the light- and heavy-labelled protein lysates of the cell lines to be compared were mixed in a 1:1 ratio, reduced, alkylated and precipitated with cold acetone. Finally, the purified protein mixtures were resuspended in loading buffer (NuPAGE™ LDS Sample Buffer, Thermo Fisher Scientific) and 40 μg of protein mix per lane were loaded on a NuPAGE™ 4–12% Bis–Tris gel (Thermo Fisher Scientific). After electrophoresis, the gel was stained with Coomassie Brilliant Blue and the gel lanes were cut into 22 slices. The gel pieces were reduced, alkylated and digested with trypsin (45). The digests were analyzed by liquid chromatography (LC)–MS/MS (PROXEON coupled to a QExactive HF mass spectrometer, ThermoFisher Scientific) with one injection of 5 μl digests. Peptides were trapped on a μPrecolumn C18 PepMap100 (5 μm, 100 Å, 300 μm × 5 mm, ThermoFisher Scientific, Reinach, Switzerland) and separated by backflush on a C18 column (5 μm, 100 Å, 75 μm × 15 cm, C18) by applying a 40-min gradient of 5% acetonitrile to 40% in water, 0.1% formic acid, at a flow rate of 350 nl/min. The Full Scan method was set with resolution at 60 000 with an automatic gain control (AGC) target of 1E06 and maximum ion injection time of 50 ms. The data-dependent method for precursor ion fragmentation was applied with the following settings: resolution 15 000, AGC of 1E05, maximum ion time of 110 ms, mass window 1.6 *m/z*, collision energy 27, under fill ratio

1%, charge exclusion of unassigned and 1+ ions, and peptide match preferred, respectively.

The mass spectrometry data was searched with MaxQuant (46) software version 1.5.4.1 against the Human Swiss-Prot (47) database (release 2016_04). Heavy labels were given as arg (R10) and lys (K8) with a maximum of three labeled amino acid in a peptide; digestion mode was set to Trypsin/P, allowing for a maximum of 2 missed cleavages; first search peptide tolerance was set to 10 ppm, and MS/MS match tolerance to 20 ppm; allowed variable modifications were Oxidation (M) and Acetyl (Protein N-term), with a maximum of 3 modifications allowed per peptide; Carbamidomethyl (C) was set as a fixed modification. Match between runs was enabled between identical gel bands and their direct neighbors with default parameters. Each pair of ratio and reversed ratio samples were analyzed to identify protein groups behaving inconsistently. This was done by plotting the log2 ratio versus the log2 inverse ratio and identification of regression outliers from absolute Studentized residuals (R MASS package (48)) >5.209 (0.9999999th quantile of the corresponding Student distribution). Protein groups flagged as outliers were not further considered. The strength of the pair correlation was then estimated using the R duplicateCorrelation package (49), and as suggested, used as parameter in the empirical Bayes approach (moderated *t*-statistics (50)) used to evaluate differential expression between the two groups. Resulting *P*-values were adjusted for multiple testing by the Benjamini and Hochberg false discovery rate-controlled approach (51).

Soft agar colony formation assay

Six-well plates were first coated with 1.5 ml of 0.5% agar dissolved in complete growing medium, and then allowed to harden for 1 h at room temperature. After the first layer was set, the top layer containing 1×10^4 cells in 1.5 ml of 0.3% agar dissolved in complete growing medium was added on top and allowed to harden for 30 min at room temperature. Plates were kept under standard cell culturing conditions for 2–3 weeks, with the regular addition of 300 µl of complete growth medium on top, to avoid drying of the plates. When treatment with NMDi was performed, the compound was added to both agar layers and to the growth medium added on top, at a final concentration of 0.3 µM. Colonies were stained for 1 hour at room temperature with crystal violet 0.01% (Sigma Aldrich) dissolved in 20% methanol and de-stained by performing several washes with water, before taking pictures with a gel documentation system. Automatic counting of the number of colonies was done using ImageJ software.

Transwell migration assay

Transwell migration assays were performed using 12-well 8 µm PET transwell inserts (Sarstedt). 1×10^4 cells were resuspended in 500 µl of FCS-free growing medium and dispensed into the upper chamber of the insert, in duplicates. The bottom well was then filled with either complete growing medium containing 10% FCS or FCS-free growing medium, which served as a control. When NMDi treatment was required, the inhibitor was added to the medium in both compartments, at a final concentration of 0.3 µM. Plates were incubated at 37°C for 20 h. Next day, non-migrating cells were removed from the upper chamber with a cotton swab and the migrated cells in the bottom side of the membrane were stained for 20 min at room temperature with crystal violet 1% in 20% methanol. After several washes with water, the membranes were cut and mounted on glass slides. Pictures of five random fields were taken, at 10x magnification, and the total number of migrated cells was counted.

Growth curves

For measuring growth rates, 6×10^4 cells/well were seeded in 12 wells of a 24-well plate in complete growth medium. Starting on the first day after seeding, the number of cells/ml present in three wells was measured every day, during 4 consecutive days. This protocol was performed in biological triplicates.

Mouse Xenograft experiments

Mouse xenograft protocols EGP 8846 and EGP 9460 were approved and executed by the MCCA Intervention Unit of the Netherlands Cancer Institute. These protocols are specifically applicable to the experiments described in this manuscript. In brief, 2×10^6 cells resuspended in Matrigel (Corning) were injected subcutaneously in the flank of NSG mice. In total, 17 mice were injected per cell line. Tumor growth was followed over time by measuring its volume with a caliper, three times per week. When the tumors reached a volume of 1500 mm³, or when animals had to be sacrificed because of their health condition, half of the tumor tissue was harvested in RNAlater (Sigma Aldrich) and stored at –80°C (for RNA extraction), and the other half was collected, fixed with formalin, and embedded in paraffin for histological examination. For the Kaplan-Meier plot, the time required for the tumors reaching 750 mm³ was taken.

Histopathological analysis of tumors

Primary tumors tissue blocks were routinely processed and stained with hematoxylin and eosin (HE) for histological examination. The primary tumors were assessed morphologically for mitotic activity and for tumor necrosis. Quantitative measurements were done digitally using QuPath 0.2.3 software. For measuring the mitotic activity, 10 high power fields of 0.237 mm² each were selected for counting mitosis. The assessment was done in the area (field of view, FOV) with estimated highest mitotic activity, selecting 10 consecutive fields. FOV with necrosis were excluded from the assessment. For the quantification of tumor necrosis, the areas of tissue with and without necrosis were measured and the percentage of necrosis was calculated.

Gelatin zymograms

Twenty µl of conditioned media collected from nearly confluent plates were mixed with 20 µl of 2× Tris-glycine SDS

sample buffer (NOVEX LC2676), in the absence of reducing agents, and incubated at room temperature for 10 min. Next, the samples were loaded onto the Novex™ 10% Zymogram Plus (Gelatin) Protein Gels (ZY00100BOX, Invitrogen) and the gel was run at 125 V using Tris-Glycine SDS running buffer. After the run was complete, the gel was incubated in Novex Zymogram Renaturing Buffer (LC2670, Invitrogen) for 30 min at room temperature, followed by a 30 min incubation in Novex Zymogram Developing Buffer (LC2671, Invitrogen). The buffer was then exchanged with fresh developing buffer and the gel was developed overnight at 37°C. Next day, the gel was stained with Imperial™ Protein Stain (Thermo Fisher Scientific) for 2 h at room temperature and then de-stained by several washes with water. Finally, gels were imaged with a gel documentation system.

Ingenuity pathway analysis

The list of differentially expressed genes between tumor samples, together with their fold changes, was uploaded to the Ingenuity Pathway Analysis (IPA) software and a core analysis was performed. Only differentially expressed genes with a fold change smaller than −2 and bigger than 2 in the comparison SMG7KO versus HT1080 were considered for this analysis. The core analysis provided the functional characterization of our dataset, from which affected diseases or biological functions were inferred. The software was used to create 'Regulators effects networks', which are functional networks that connect differentially expressed genes (DEGs) with both downstream effects and upstream regulators. The IPA software was also used to compare the DEGs and the predicted downstream effects of the RNAseq data from the tumor samples and the one of the cells in culture.

Graphs and statistical analysis

All graphs and statistical analysis were done with GraphPad Prism 9 software. The graphical abstract was created with Biorender.com.

RESULTS

Lack of SMG7 results in strong NMD inhibition

The reported pro- and anti-carcinogenic roles of NMD prompted us to investigate the impact of the NMD factor SMG7 in the tumorigenicity of a human fibrosarcoma model. To this end, we generated SMG7 knockout cells in the human fibrosarcoma-derived cell line HT1080 (SMG7KO) by applying CRISPR-Cas9 genome editing to introduce a gene trap (consisting of a splicing acceptor (SA), a Zeocin resistance cassette (Zeo^R) and a strong polyadenylation signal (PA)) into the first intron of the SMG7 gene (Figure 1A) (42). In cell clones bearing the correct integration of the gene trap in both alleles, transcription of the SMG7 locus confers Zeocin resistance but no SMG7 expression, as transcription should stop at the integrated SV40 polyadenylation motif. We used western blotting (WB) to confirm the absence of both the short and the long protein isoforms of SMG7 in two independently generated SMG7KO clones (clones 11 and 12, Figure 1B) and RNA sequencing (RNAseq) to verify that there

are no reads mapping to the SMG7 locus downstream of the integrated gene trap (42). To assess if SMG7KO cells have impaired NMD, we performed differential gene expression analysis on the RNAseq data previously generated for the SMG7KO clones 11 and 12 and for the parental cell line HT1080 (Figure 1C and Supplementary Table S1) (42). The changes in the transcriptome observed in both SMG7KO clones correlate with each other (Pearson correlation $R = 0.9248$), suggesting that they are not specific to either clone but rather common to the loss of SMG7. In total, 3400 genes were found to be differentially expressed (DEG, meta adjusted P-value < 0.01), of which 1763 were upregulated and 1637 were downregulated in SMG7KO cells. Given the role of SMG7 in RNA decay, it was surprising to find such a big fraction of downregulated genes. We reasoned that the changes in gene expression observed in SMG7KO cells are the sum of both direct and indirect (or secondary) effects of the lack of SMG7. If in addition we apply a fold change cutoff of ± 1.5, we find that 2867 genes are differentially expressed, with 1524 of them being upregulated and 1343 downregulated in SMG7KO cells compared to parental HT1080 cells. Among the upregulated genes, we find well validated NMD substrates like GADD45B, GAS5 (Supplementary Table S1) and genes encoding NMD factors (Supplementary Table S1 and Figure 1C), as part of the NMD autoregulatory mechanism (9,10,18), further confirming that NMD is impaired in SMG7KO cells. In addition, we wondered if the NMD inhibition observed in SMG7KO cells could also impact their proteome. To answer this, we did a quantitative proteomic analysis on both SMG7KO clones and on parental HT1080 cells using stable isotope labeling by amino acids in cell culture (SILAC) and mass spectrometry (Supplementary Figure S1A and Supplementary Table S2). The protein expression changes observed in both SMG7KO clones relative to HT1080 cells also correlate with each other (Pearson correlation $R = 0.6770$), and among the top upregulated proteins we found many NMD factors, like UPF1, UPF2, SMG1 and SMG9 (Supplementary Figure S1A). In summary, our transcriptomic and proteomic analyses document a strong NMD impairment in the SMG7KO cells.

Next, we generated a RESCUE cell line in which we re-introduced both isoforms of SMG7 into the SMG7KO clone 12 (from now on termed SMG7KO, for simplicity). Compared to isoform 1, isoform 2 lacks amino acids 569–614 due to alternative pre-mRNA splicing but thus far no functional differences between the two isoforms have been reported. We used RT-qPCR to evaluate SMG7 expression and NMD activity in SMG7KO clones 11 and 12, the RESCUE cell line and in the parental cells HT1080. Analysis of SMG7 levels (Figure 1D) confirmed that SMG7KO clones do not express any detectable amounts of SMG7 mRNA and that this has been restored in the RESCUE cells, results that agree with our RNAseq data and with the SMG7 protein levels detected by WB (Figure 1B). Our RT-qPCR analysis further confirmed the specific accumulation of endogenous NMD-sensitive mRNAs in SMG7KO cells and revealed that their levels are brought back to that of the HT1080 cells in the RESCUE condition, suggesting that NMD activity has been fully restored in the RESCUE cells (Figure 1E, F and Supplementary
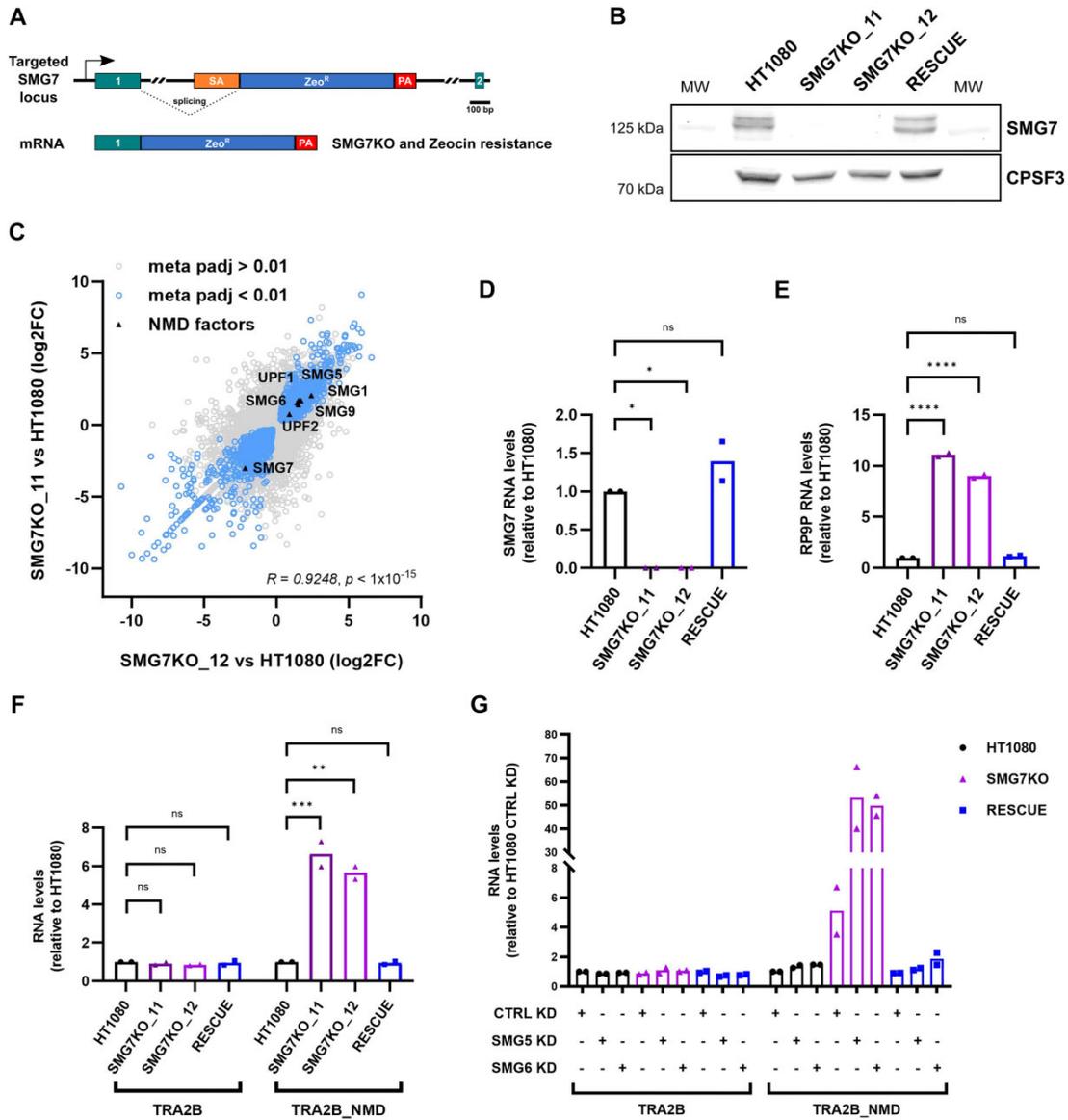
Figure 1. SMG7KO cells have impaired NMD. (**A**) Scheme of the genome editing approach used to generate the SMG7KO cell lines. A gene trap consisting of a splicing acceptor (SA), a Zeocin resistance cassette (Zeo^R) and a strong polyadenylation signal (PA) was inserted into the first intron of the SMG7 gene. The first two exons of the SMG7 gene are shown in green. (**B**) Western blot showing the levels of SMG7 protein in HT1080, SMG7KO clones 11 and 12, and the RESCUE cell lines. Both isoforms of SMG7 are distinguishable, CPSF3 serves as a loading control. MW: molecular weight marker. (**C**) Scatter plot showing the correlation between the differential gene expression analyses performed on RNAseq data from SMG7KO clones 11 and 12 compared to the parental cell line HT1080. The Pearson correlation coefficient (*R*) calculated for the differentially expressed genes (DEG, in blue) with meta adjusted *P*-values (meta P_{adj}) < 0.01 is shown. The DEGs encoding NMD factors are shown in black. (**D–F**) Relative mRNA levels were determined by RT-qPCR and normalized to the average of the relative levels of ActB mRNA and 28S rRNA. Shown are the means and data points represent biological replicates. Statistical significance was determined by One-way ANOVA and Dunnett's multiple comparisons test. *ns* $P > 0.05$; * $P \leq 0.05$; ** $P \leq 0.01$; *** $P \leq 0.001$; **** $P \leq 0.0001$. (**G**) Relative mRNA levels, determined by RT-qPCR as in (D), in HT1080, SMG7KO_12 and the RESCUE cell lines treated with the indicated siRNAs. Shown are the means and data points represent biological replicates.

Figure S1B-C). The model proposing that SMG5 and SMG7 proteins are required to form a heterodimer to trigger mRNA decay (16) was recently challenged by two publications providing evidence that SMG5 and SMG7 can have heterodimer-independent functions in NMD (12,17). We reasoned that our cell lines provide a good framework to examine these new findings. We performed siRNA-mediated knock downs (KD) of SMG5 and SMG6 in HT1080, SMG7KO and RESCUE cells and we evaluated NMD activity by RT-qPCR. Indeed, we found that in cells lacking SMG7, depletion of SMG5 led to an even stronger NMD inhibition (Figure 1G and Supplementary Figure S1D–F), further supporting the idea that SMG5 can sustain NMD activity in the absence of SMG7. A similar picture was observed when SMG6 was depleted from SMG7KO cells, results that can be explained by the concomitant inhibition of both mRNA decay branches, as it has been reported previously (10,12). We were reassured to see that the accumulation of NMD substrates upon depletion of SMG5 or SMG6 in the RESCUE cells was similar to that of the parental HT1080 cells, showing that the expressed recombinant SMG7 proteins are fully functional.

NMD inhibition affects the anchorage-independent growth and migration properties of HT1080 cells

Due to their highly aggressive and invasive nature, the HT1080 cells have been used extensively as a model for studying cell invasion and migration (52–55). Given the wealth of conflicting data relating NMD and tumorigenesis (21), we decided to study if the tumorigenic potential of the HT1080 cells is affected by the loss of SMG7. First, we compared the anchorage-independent growth abilities of parental, SMG7KO and RESCUE HT1080 cells by performing soft agar colony formation assays and found that the SMG7KO cells show a four-fold reduction in the number of colonies they form, when compared to HT1080 and RESCUE cells (Figure 2A). We did not, however, find differences in the growth rates of the cell lines under standard adherent cell culturing (Supplementary Figure S2A). Similar results were obtained with another SMG7KO clone, number 11 (Supplementary Figure S2B), suggesting that this is not a clone-specific trait. Additionally, we wanted to assess if the impaired ability to grow in the absence of a solid surface is a feature attributable to the lack of SMG7, or more generally to NMD inhibition. For this, we performed soft agar colony formation assays on HT1080 cells treated with a small molecule drug (NMDi) that blocks NMD by inhibiting the kinase activity of SMG1 (56,57), and observed that the NMDi treatment also significantly reduces the capacity of HT1080 cells to form colonies in soft agar (Figure 2A).

Next, we performed transwell migration assays to compare the migratory properties of the cell lines, using fetal calf serum (FCS) as a chemoattractant. We found that the number of migrating cells was significantly reduced for the SMG7KO cell line, compared to HT1080 and RESCUE cells (Figure 2B). Comparable results were obtained when HT1080 cells were treated with the NMDi, suggesting that NMD inhibition causes the impaired migratory capacity of the SMG7KO cells. In summary, our results show that the anchorage-independent growth and migratory abilities of HT1080 cells are impaired when NMD activity is compromised.

SMG7KO cells show impaired tumorigenicity *in vivo*

The results obtained in our cell-based assays led us to hypothesize that SMG7KO cells might have difficulties in forming tumors *in vivo*. To test this, we performed mouse xenograft experiments in which parental, SMG7KO and RESCUE HT1080 cells were injected subcutaneously into immunocompromised mice and tumor growth was measured over time with a caliper. The results are summarized in figures 3A and B. Tumor growth was detected in all mice injected with the parental HT1080 cells, and most of these tumors reached a volume of 750 mm^3 within about 50 days after injection (15/17, ~88% of total) (Figure 3A, B). On the contrary, tumors formed by the SMG7KO cells grew more slowly (Figure 3A). In ~35% (6/17) of the injected animals we couldn't find evidence of tumor growth, and from the ~65% (11/17) of the cases in which tumor growth was detectable, only 4 of them (~24% of total) reached a volume of 750 mm^3 within the timeframe of the experiment (Figure 3B). RESCUE cells were also able to form tumors *in vivo*, albeit at a slower speed than that of parental HT1080 cells (Figure 3A). There was also a fraction of RESCUE-injected mice for which tumor growth wasn't detectable (4/17, ~24%), however, in contrast to the SMG7KO cells, a large proportion of the tumors formed by RESCUE cells reached a volume of 750 mm^3 (10/17, ~59% of total) (Figure 3B).

To further characterize the tumors formed by the three cell lines, we performed a histopathological analysis of the primary tumors, which were assessed morphologically, for mitotic activity and for tumor necrosis. Based on the predominant tumor shape and the extent as well as the distribution of necrosis, the tumors demonstrated one of the following main morphologies: (a) highly and densely cellular, multinodular, space-occupying mass, with frequent focally-extensive epidermal and dermal necrosis on the surface (infarct), and variable intratumoral necrosis; (b) highly and densely cellular, multinodular, plaque-like more than space-occupying mass with massive central focally-extensive necrosis; (c) plaque-like mass with >80% necrotic tumor tissue with evident dissociated neoplastic cells (Figure 3C). Some cases presented with an intermediate morphology of (a) and (b), characterized by a combination of histomorphological features from both groups. Morphology (a) was clearly predominating in the HT1080 (75%) and RESCUE (70%) groups. For the SMG7KO group, however, none of the morphologies predominated clearly over the others, with morphology (c) being the most frequently found (Figure 3D). The more plaque-like and smaller appearing tumors may correspond to slower growing neoplasias compared to the larger, multinodular, and more expansive tumors. Additionally, the extent of tumor necrosis may also potentially correspond to reduced tumor growth as the extent of necrotic lesions would be expected to increase with prolonged presence and development of the tumors. The quantification of the mitotic activity, as well as the percentage of necrosis in the primary tumors
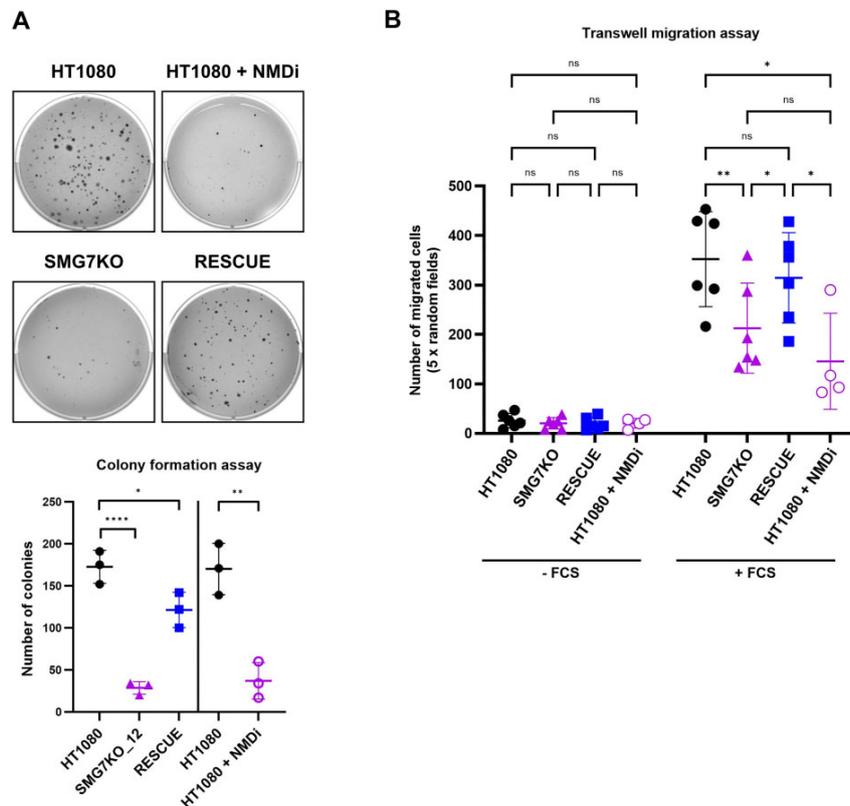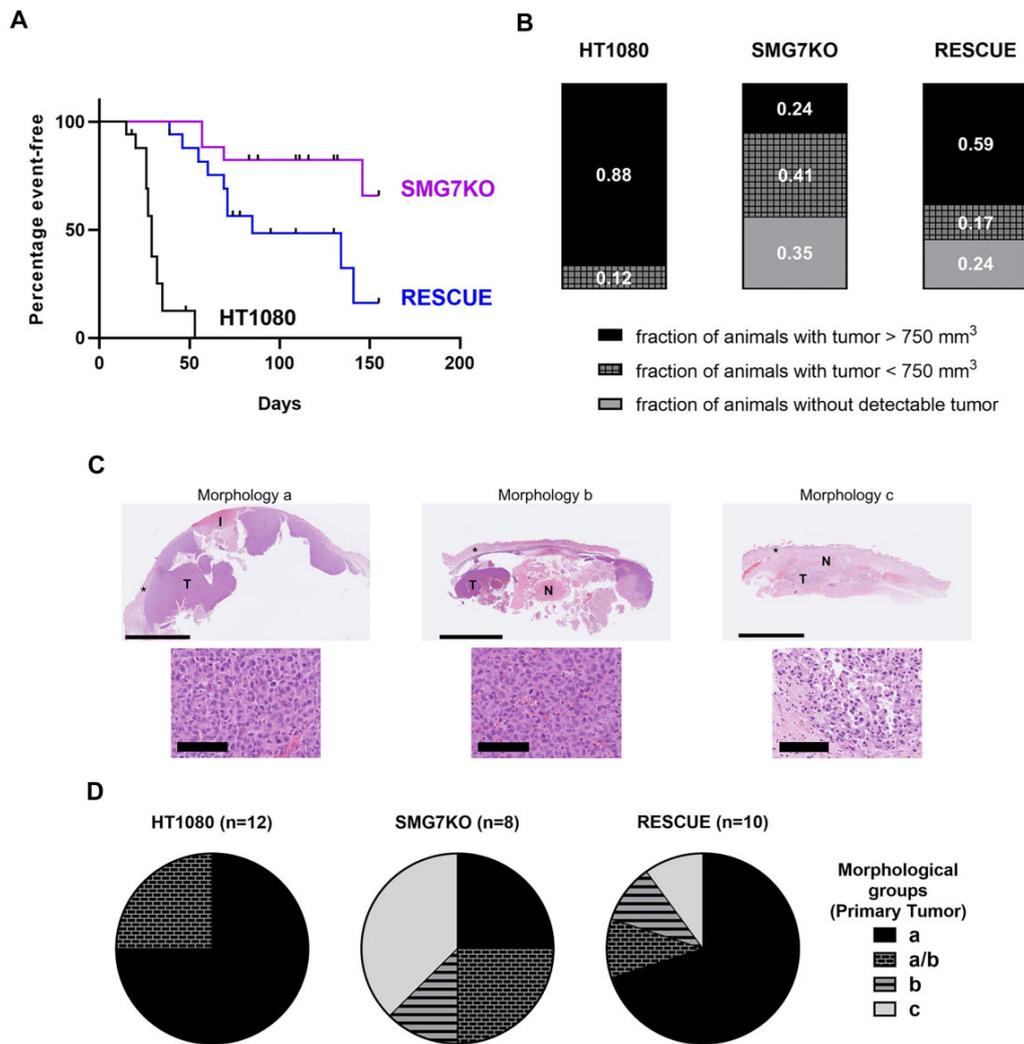
Figure 2. SMG7KO cells show impaired migration and anchorage-independent growth. (**A**) Soft agar colony formation assays were used to determine the anchorage-independent growth properties of HT1080, SMG7KO and RESCUE cell lines, and of HT1080 cells treated with an NMD inhibitor (NMDi, 0.3 μM) as an alternative way of inhibiting NMD. Top panel, representative images of colonies stained with crystal violet. Bottom panel, quantification of the colony formation assays, showing the number of colonies per well and the means ± SD of three biological replicates for the indicated cell lines and treatments. Statistical significance between HT1080, SMG7KO_12 and RESCUE cells was determined by One-way ANOVA and Dunnett's multiple comparisons test, * $P \leq 0.05$; **** $P \leq 0.0001$. Statistical comparison of HT1080 and HT1080 + NMDi cells was performed by unpaired two-tailed *t*-test, ** $P \leq 0.01$. (**B**) Results of transwell migration assays performed with HT1080, SMG7KO and RESCUE cell lines, and with NMDi-treated (0.3 μM) HT1080 cells. Data points represent the number of migrated cells from five randomly chosen fields of the membranes in each biological replicate. Additionally, the means ± SD are shown. Statistical significance was determined by Mixed-effects analysis and Tukey's multiple comparisons test. *ns* $P > 0.05$; * $P \leq 0.05$; ** $P \leq 0.01$.

support this idea: the mitotic activity of the primary tumors was highest in the HT1080 group, lowest in the SMG7KO group and intermediate for the RESCUE group (Supplementary Figure S3A). The opposite trend was observed for the quantification of tumor necrosis, which was highest in the SMG7KO group and lowest for the HT1080 group, with intermediate values for the RESCUE group (Supplementary Figure S3B). Even though these differences in mitotic activity and necrosis did not reach statistical significance, they suggest that the tumors formed by SMG7KO cells grew more slowly than those formed by parental HT1080 cells, and that this phenotype was partially reverted in the RESCUE cells. Finally, we reconfirmed the identity of the cells present in the primary tumors by measuring SMG7 mRNA levels by qPCR (Supplementary Figure S3C). Altogether, our results show that the high tumorigenicity characteristic of HT1080 cells was reduced in the SMG7KO cells, and that this attribute was partially restored in the RESCUE cells.

NMD inhibition results in reduced MMP9 gene expression in HT1080 cells

To get more insight into the molecular mechanisms responsible for the impaired tumorigenicity of the SMG7KO cells, we performed RNAseq and differential gene expression analysis on primary tumors formed by parental, SMG7KO and RESCUE HT1080 cells (Figure 4A and Supplementary Table S3). The anti-correlation observed when plotting the DEGs (defined by having an adjusted *P*-value <0.01 in either of the two pairwise comparisons) between SMG7KO and HT1080 cells (*x* axis) versus the DEGs between RESCUE and SMG7KO cells (*y* axis) suggests that many of the transcriptomic changes induced by the removal of SMG7 have been restored in the RESCUE cells (Pearson correlation *R* = –0.6176; Figure 4A). Again, as a paradigm of NMD inhibition, we verified the accumulation of the NMD sensitive mRNAs encoding for the NMD factors UPF1, SMG1, SMG5 and SMG9 in the tumors formed by SMG7KO cells, and we also confirmed that their levels are

Figure 3. SMG7KO cells show impaired tumorigenicity *in vivo*. (**A**) Kaplan–Meier plots showing tumor progression in mice with HT1080, SMG7KO and RESCUE xenografts. The endpoint (event) was defined as tumors reaching a volume of 750 mm³. Black ticks represent censored animals. Each group consisted of 17 mice. Survival curves were compared using the Log-rank (Mantel-Cox) test (HT1080 versus SMG7KO, and HT1080 versus RESCUE $P < 0.0001$, SMG7KO versus RESCUE $P = 0.0149$). (**B**) For the Xenograft experiment shown in A, the fraction of animals that did not develop a detectable tumor during 150 days after injection of the cells (gray), animals with tumors smaller than 750 mm³ (gridded) and animals for which the tumors reached at least 750 mm³ (black) is shown. (**C**) Hematoxylin and eosin (H&E) staining was used for histological examination of the primary tumors. Shown are representative images of the three distinctive morphological groups termed a, b and c. The overview images (top) were taken at 0.6× and the scale bar corresponds to 5 mm. 'T' denotes viable tumor tissue, 'N' shows necrotic tissue and the asterisks show the skin. 'I' indicates the dermal necrosis (infarct), characteristic of tumors belonging to group a. The close-up images (bottom) were taken at 25× and the scale bar corresponds to 100 μm. The dissociation of the neoplastic cells is evident in tumors from group c. (**D**) Pie charts showing the proportion of the tumors formed by HT1080, SMG7KO and RESCUE cells that were classified into one of the three main morphological groups (a, b or c). The fourth category labeled a/b corresponds to tumors containing features of both categories. The total number of primary tumors analyzed per cell line is indicated between parentheses.

again downregulated in the tumors established from RES-CUE cells (Figure 4A).

We then used the Ingenuity Pathway Analysis (IPA) software to perform a functional analysis on the RNAseq data of the primary tumors. Using the 'Downstream effects' analysis tool, which uses the gene expression changes in the dataset to predict which biological processes or functions might be activated or inhibited, we found categories like 'Invasion of cells', 'Advanced malignant tumor', 'Invasive tumor', and 'Metastasis' to be inhibited in the tumors

formed by SMG7KO cells (z-scores < -2) (Supplementary Figure S4A), a result that is consistent with the observed phenotype. In addition, we implemented a 'Regulator effects' analysis to get insight into the upstream regulators and the DEGs that might be driving the predicted downstream effects. This analysis resulted in only one causal network with a positive consistency score (a measure of how causally consistent and densely connected the network is) that connects 13 DEGs that are predicted to contribute to the inhibition of the categories 'Migration of cells',
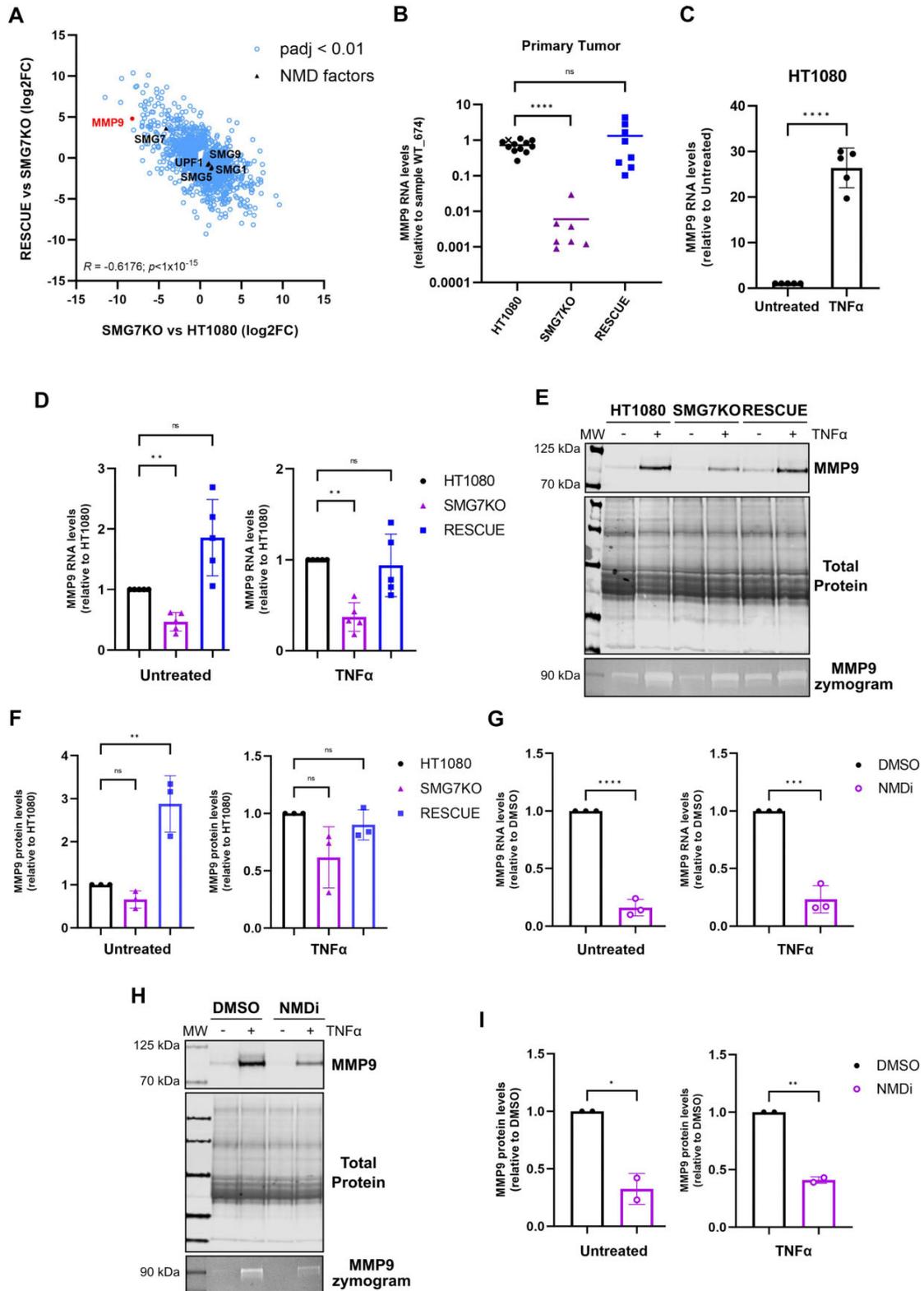
Figure 4. NMD inhibition leads to decreased MMP9 expression. (**A**) Scatter plot showing the pairwise differential gene expression analyses performed on RNAseq data from primary tumors. DEGs between SMG7KO and HT1080 cells are plotted along the *x* axis, and those between RESCUE and

'Invasion of cells' and 'Metastasis' (Supplementary Figure S4B). We also used the 'Comparison' tool from the IPA software to study which DEGs and downstream affected diseases or functions are shared between the RNAseq data from the primary tumors and that of the cells in culture. We found that the gene expression changes observed in the cultured cells also suggested the inhibition of categories like 'Invasion of cells', 'Metastasis' and 'Advanced malignant tumor' in the absence of SMG7 (Supplementary Figure S4C).

Among the DEGs reported to affect these downstream categories, we found Matrix Metallopeptidase 9 (MMP9; also known as 92 kDa Gelatinase) to be a very interesting candidate for further study. MMP9 9 is a proteinase that degrades type IV and V collagens and its activity has been suggested to play a role in extracellular matrix remodeling during tumorigenesis (58–60). MMP9 is among the most downregulated genes in the tumors formed by SMG7KO cells and its expression is reestablished in the RESCUE tumors (Figure 4A), results that were further validated by analyzing MMP9 mRNA levels in the primary tumors by RT-qPCR (Figure 4B). The transcriptomic analysis from the cells in culture also showed that MMP9 gene expression is downregulated in the SMG7KO cells (SMG7KO_12 log2FC: -3.85; SMG7KO_11 log2FC: -2.51). The expression level of MMP9 in the cultured cells is, however, quite low, and we therefore used TNFα stimulation, which induces MMP9 expression by about 25-fold (Figure 4C). We compared the levels of MMP9 mRNA in HT1080, SMG7KO and RESCUE cells by RT-qPCR and found that, either untreated or after TNFα stimulation, SMG7KO cells consistently expressed less MMP9 mRNA than HT1080 and RESCUE cells (Figure 4D). We confirmed that the downregulation in MMP9 mRNA levels also results in less secreted MMP9 protein and, consequently, less gelatinolytic activity detected in conditioned media from SMG7KO cells (Figure 4E, F). To understand if the observed downregulation of MMP9 levels can be attributed to NMD inhibition,

we analyzed the expression levels and activity of MMP9 in HT1080 cells treated with the NMDi and found that this alternative way of inhibiting NMD also resulted in downregulation of MMP9 expression (Figure 4G–I and Supplementary Figure S4D). Furthermore, we also observed diminished MMP9 expression in HT1080 cells depleted of the core NMD factor UPF1 (Supplementary Figure S4E–G). In summary, our results show that NMD inhibition results in reduced expression of the MMP9 gene in HT1080 cells.

MMP9 overexpression improves the anchorage-independent growth and migration capacities of SMG7KO cells

MMP9 expression has been suggested to directly impact cell invasion, migration, and metastasis in a variety of cell lines and model organisms (59,61–64). Given the direct implication of MMP9 in these essential processes for tumorigenicity, we wanted to test if increasing MMP9 expression in SMG7KO cells could rescue some of the phenotypes we described above. We genome-edited the SMG7KO cells to overexpress a C-terminally FLAG-tagged version of MMP9, a cell line we refer to as MMP9OE. We confirmed that the recombinant protein is expressed in high quantities, it is secreted into the conditioned medium and it is active in degrading gelatin (Figure 5A, B). We next compared the migration properties of SMG7KO and MMP9OE cells by doing transwell migration assays and found that MMP9OE cells show increased migration compared to SMG7KO cells (Figure 5C). We also performed colony formation assays and found that MMP9 overexpression partially rescues the soft-agar growth impairment of the SMG7KO cells (Figure 5D). Overall, we found that the defects in anchorage-independent growth and migration capacities caused by NMD inhibition in the HT1080 cells can be partially rescued by overexpression of MMP9.

Next, we decided to investigate if the decrease in MMP9 expression upon NMD inhibition results from transcriptional changes, or rather from changes in the stability of the

SMG7KO cells along the *y* axis. Only differentially expressed genes with an adjusted *P*-value ($P_{adj} < 0.01$) in either of the two comparisons are plotted (in blue), and the Pearson correlation coefficient (*R*) for them is shown. The genes encoding NMD factors are shown in black and the MMP9 gene is shown in red. (**B**) MMP9 gene expression in primary tumors. Relative MMP9 mRNA levels were determined by RT-qPCR, normalized to ActB mRNA, and expressed relative to the tumor sample HT1080_674, marked with a 'x'. Each data point represents the result of a different primary tumor and the mean values are indicated. Statistical significance was determined by unpaired two-tailed t-test. *ns p* > 0.05; **** $P \le 0.0001$. (**C**) Relative MMP9 mRNA levels in HT1080 cells untreated or treated with TNFα (25 ng/ml). MMP9 expression was determined by RT-qPCR, normalized to ActB mRNA and 28S rRNA. Shown are the means ± SD and data points represent biological replicates. Statistical significance was determined by unpaired two-tailed t-test. **** $P \le 0.0001$. (**D**) Relative MMP9 mRNA levels in HT1080, SMG7KO and RESCUE cells untreated or treated with TNFα (25 ng/ml). MMP9 expression was determined by RT-qPCR, normalized to ActB mRNA and 28S rRNA. Shown are the means ± SD and data points represent biological replicates. Statistical significance was determined by One-way ANOVA and Dunnett's multiple comparisons test. *ns p* > 0.05; ** $P \le 0.01$. (**E**) Analysis of MMP9 protein expression and activity. Western Blot was used to analyze the levels of MMP9 protein present in conditioned medium collected from HT1080, SMG7KO and RESCUE cells untreated or treated with TNFα (25 ng/ml). Total protein staining serves as a loading control. Lower panel: gelatin zymography was used to detect the gelatinolytic activity of secreted MMP9. (**F**) Densitometric quantification of secreted MMP9 protein levels detected by western blot from HT1080, SMG7KO and RESCUE cells, untreated or treated with TNFα (25 ng/ml). MMP9 levels were normalized to total protein amounts, results of three biological replicates and the means ± SD thereof are shown. Statistical significance was determined by One-way ANOVA and Dunnett's multiple comparisons test. *ns P* > 0.05; ** $P \le 0.01$. (**G**) Relative MMP9 mRNA levels in HT1080 cells treated with DMSO or with the NMD inhibitor (0.3 µM) in the absence or presence of TNFα (25 ng/ml). MMP9 expression was determined by RT-qPCR, normalized to ActB mRNA and 28S rRNA. Shown are the means ± SD and data points represent biological replicates. Statistical significance was determined by unpaired two-tailed *t*-test. *** $P \le 0.001$; **** $P \le 0.0001$. (**H**) Analysis of MMP9 protein expression and activity. Western Blot was used to analyze the levels of MMP9 protein present in conditioned medium collected from HT1080 cells treated with DMSO or with the NMD inhibitor (0.3 µM) in the absence or presence of TNFα (25 ng/ml). Total protein staining serves as a loading control. Lower panel: gelatin zymography was used to detect the gelatinolytic activity of secreted MMP9. (**I**) Densitometric quantification of secreted MMP9 protein levels detected by western blot from HT1080 cells treated with DMSO or with 0.3 µM NMDi in the absence or presence of TNFα (25 ng/ml). MMP9 levels of two biological replicates were quantified and are displayed as in (F). Statistical significance was determined by unpaired *t*-test. * $P \le 0.05$; ** $P \le 0.01$.
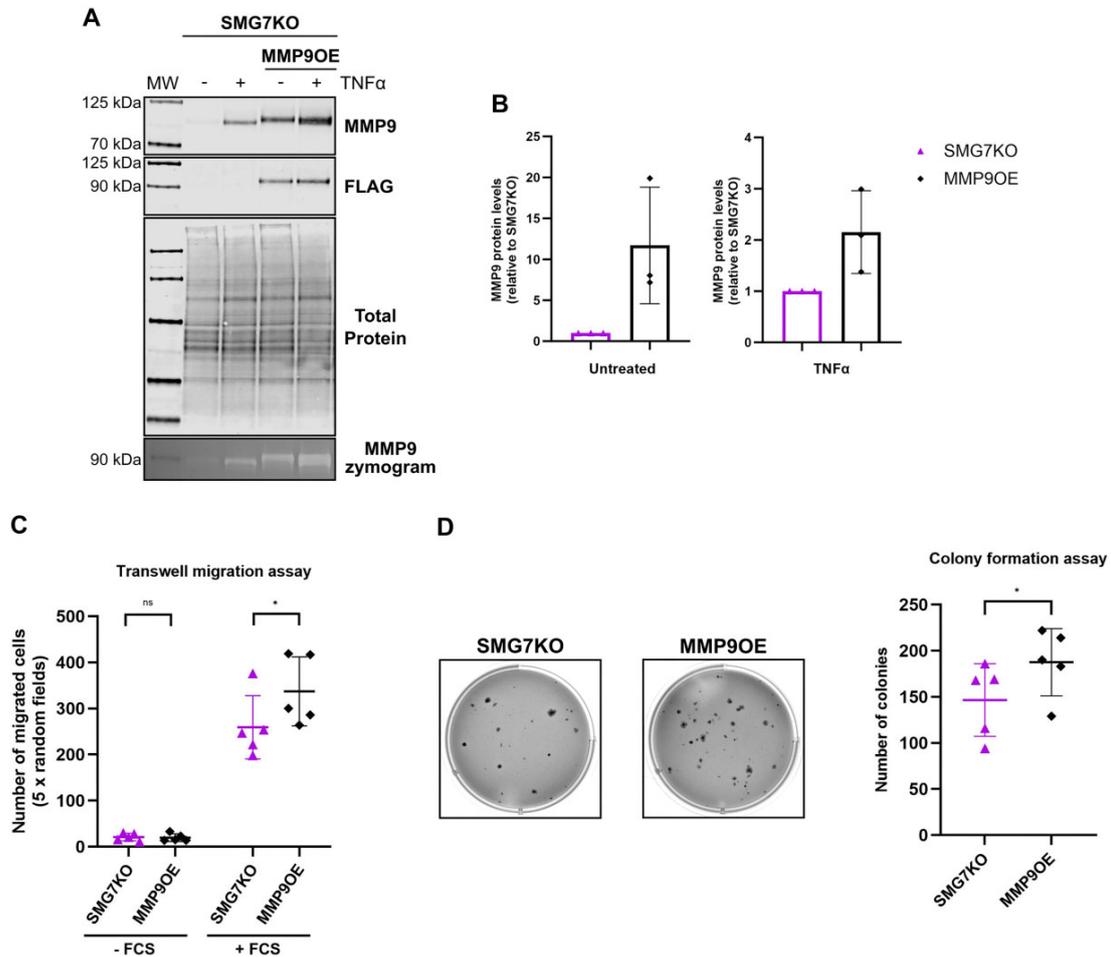
Figure 5. MMP9 overexpression improves the anchorage-independent growth and migratory properties of SMG7KO cells. (**A**) Analysis of MMP9 protein expression and activity. Western Blot was used to analyze the levels of MMP9 protein present in conditioned medium collected from SMG7KO and MMP9OE cells untreated or treated with TNFα (25 ng/ml). Anti-FLAG antibody detects only the recombinant MMP9. Total protein staining serves as a loading control. Lower panel: gelatin zymography was used to detect the gelatinolytic activity of secreted MMP9. (**B**) Densitometric quantification of secreted MMP9 protein levels detected by western blot from conditions shown in (A). MMP9 levels of three biological replicates were quantified the means ± SD thereof are shown. (**C**) Results of transwell migration assays performed with the SMG7KO and MMP9OE cell lines. Data points represent the number of migrated cells from five randomly chosen fields of the membranes in each of the five biological replicates. Shown are the means ± SD and statistical significance was determined by paired two-tailed *t*-tests. *ns* $P > 0.05$; * $P \leq 0.05$. (**D**) Soft agar colony formation assays were used to compare the anchorage-independent growth properties of SMG7KO and MMP9OE cell lines. The number of colonies formed by each cell line was quantified and the right panel shows the results of each of the five biological replicates and the means ± SD thereof. Statistical significance was determined by paired two-tailed *t*-test. * $P \leq 0.05$.

transcript. To answer these questions, we quantified MMP9 mRNA and pre-mRNA levels by RT-qPCR, in HT1080 cells treated with DMSO or NMDi in the absence or presence of TNFα. We observed that the levels of both MMP9 mRNA and pre-mRNA are decreased to similar extents in NMD inhibited cells, compared to DMSO-treated cells (Supplementary Figure S5A). We also studied the kinetics of the accumulation of the MMP9 mRNA and pre-mRNA in HT1080 cells depleted of UPF1, after TNFα stimulation of MMP9 transcription. In cells undergoing a CTRL KD, we found that MMP9 pre-mRNA levels are increased already after 1 hour of TNFα stimulation, whereas MMP9 mRNA accumulation is only detected at least two h later (Supplementary Figure S5B), suggesting that com-

plete transcription of the MMP9 locus and/or processing of the MMP9 mRNA is a lengthy process. Compared to CTRL KD cells, UPF1-depleted cells consistently express less MMP9 mRNA and pre-mRNA throughout the TNFα time-course (Supplementary Figure S5B). Collectively, these results suggest that NMD inhibition leads to decreased transcription of the MMP9 gene. We also explored the possibility that the stability of the MMP9 mRNA might be affected by NMD inhibition. We induced MMP9 expression by TNFα treatment for 24 h and then treated the cells with Actinomycin D (ActD), to stop transcription. At different time points after ActD addition, the levels of MMP9 mRNA were determined by RT-qPCR. We observed that the stability of the MMP9 mRNA is very

similar in HT1080 cells treated with DMSO or NMDi (Supplementary Figure S5C). As controls, we confirmed that the NMD-sensitive TRA2B_NMD transcript was completely stabilized upon NMDi treatment, whereas the stability of the NMD-insensitive protein coding TRA2B isoform was not affected by NMDi (Supplementary Figure S5C).

Finally, we wondered if the reduced expression of MMP9 under NMD inhibition stems from a failure of these cells to respond to TNFα. To answer this question, we analyzed the expression of the two TNFα early-response genes A20 and NFKBIA (65) after 1 h of TNFα stimulation. We did not find differences in the induction of these genes in UPF1-depleted cells, compared to a control knockdown in HT1080 cells (Supplementary Figure S5D), or between HT1080, SMG7KO, and RESCUE cells (Supplementary Figure S5E). We therefore conclude that the failure to upregulate MMP9 cannot be explained by a general insensitivity to TNFα in NMD-inhibited cells. Collectively, our results suggest that NMD inhibition results in decreased transcription of the MMP9 gene and that MMP9 overexpression partially rescues the oncogenic phenotype in SMG7KO cells.

DISCUSSION

In mammalian cells, NMD is an essential RNA degradation pathway, with a continuously growing list of reported roles in cellular physiology (19). Among these, evidence for different impacts of NMD on tumor development has emerged over the past years, with examples ranging from NMD benefitting tumor growth to NMD inactivation being specifically associated with tumor tissue (21). Here, we used the human fibrosarcoma cell line HT1080 to investigate the roles of the NMD factor SMG7 in tumorigenesis. Using CRISPR-Cas9-based approaches, we generated SMG7KO cells and its RESCUE counterpart, and we confirmed that NMD activity is strongly inhibited in the former and restored in the latter (Figure 1 and Supplementary Figure S1). We found that the NMD-inhibited SMG7KO cells show impaired cell migration and clonogenic abilities (Figure 2 and Supplementary Figure S2), and that they display severe delays when challenged to form tumors *in vivo* (Figure 3 and Supplementary Figure S3). Gene expression analysis showed that NMD-inhibited cells fail to upregulate the expression of the pro-tumorigenic gene MMP9 both *in vivo* and in cell culture (Figure 4 and Supplementary Figure S4). Finally, we showed that restoring MMP9 expression in SMG7KO cells partially rescues their clonogenicity and migration properties (Figure 5 and Supplementary Figure S5). Collectively, our work shows in this fibrosarcoma model, that the tumor cells depend on NMD to exert their tumorigenic properties.

Since the realization that NMD targets for degradation not only faulty mRNAs but also mRNAs with full coding potential (for a comprehensive list see (66,67)), there has been a longstanding quest to identify cellular functions and pathways that are susceptible to changes in NMD activity (19,68). Efforts to answer these questions in mammalian cells included RNAi-mediated transient KD experiments (10,69,70) and, more recently, generation of complete KOs of NMD factors (12,17,71,72). The commonly used

strategy for generating KOs by introducing Cas9-driven indels in the coding region of a gene, which will in most cases lead to a frameshift and a premature termination codon, relies on the NMD pathway to destroy the mutant mRNA. This editing strategy therefore might not be well suited when the target gene encodes an NMD factor, because NMD inhibition would result in stabilization of the mutant mRNA, allowing for translation of truncated versions of the protein that could have deleterious or unforeseen effects on cells. By contrast, the CRISPR-Trap approach (42) overcomes this caveat and proved to be very efficient in allowing the stable and complete removal of the SMG7 mRNA and protein. This KO of SMG7, in turn, uncovered the profound effect that SMG7 depletion has on the transcriptome of human cells, which contrasts with the mild phenotypes obtained previously for SMG7 KD experiments (9,10,12). This discrepancy can have two non-mutually exclusive explanations: on the one hand, the temporal distinction between transient KDs and stable KOs may account for the differences in the magnitude and the number of deregulated genes; on the other hand, it is conceivable that low residual levels of SMG7 can still sustain NMD activity in transient KD experiments and that this can only be surpassed when SMG7 is completely ablated from the cells. Our work reinforces the recent findings that SMG5 and SMG7 can have heterodimer-independent roles in NMD (12,17). Specifically, we showed that in the absence of SMG7, SMG5 is still engaged in sustaining NMD activity, as evidenced by the strong upregulation of NMD substrates when SMG5 was depleted from SMG7KO cells. The extent to which NMD substrates accumulated in SMG7KO/SMG5KD and SMG7KO/SMG6KD conditions was remarkably similar, suggesting that both combinations lead to a comparable level of NMD inhibition. These results agree with the notion that the concomitant depletion of SMG5 and SMG7 also affects the activity of the endonucleolytic SMG6-mediated mRNA decay, as recently reported (12), and with the fact that the level of NMD inhibition achieved by the co-depletion of SMG5 and SMG7 is not further increased by the depletion of all three NMD effectors simultaneously (12,17).

It is well established that the accumulation of somatic genetic alterations drives the development of cancer (73). Consequently, cancer cells express more PTC-bearing mRNAs compared to non-cancerous cells because of such frameshifting or nonsense mutations. The impact of these mutations on cancer fitness depends not only on whether they are driver mutations occurring in oncogenes or tumor suppressor genes, or passenger mutations that do not confer a growth advantage to the tumor cells, but also on whether they are targeted by NMD and, if they are, to which extent. Tumor evolution is a Darwinian process, and genome-wide studies have highlighted how the selective pressure has shaped the mutational landscape and NMD activities of tumor cells to benefit cancer development. Pan-cancer studies have shown that tumor suppressor genes preferentially accumulate NMD-eliciting mutations, whereas oncogenes are under purifying selection against mutations that trigger NMD (29,30). Furthermore, it has been reported that the core NMD factor genes are amplified in diverse tumor types, and that this correlates with increased NMD

efficiency and lower cytolytic activity (31), suggesting that enhanced NMD activity might be beneficial for tumor growth. In addition, NMD activity can be instrumental for cancers to evade the immune response. mRNAs containing frameshift mutations, if translated, can give rise to novel peptides that can be recognized as neoantigens by the immune system and trigger an anti-tumor response. However, NMD can limit the expression of neoantigens by degrading the mutant mRNAs (24,26,74). It has been reported that cancers with a high frequency of NMD-insensitive frameshift mutations show increased immune infiltration and are associated with a better outcome after treatment with immune checkpoint inhibitors (27,28). Consistent with this, NMD inhibition results in strong immune responses and reduced tumor growth *in vivo* (22–25). Our findings that NMD inhibition results in decreased tumorigenicity in the HT1080 fibrosarcoma model is fully in line with these reports and with a very recent publication showing the critical role of SMG7 in the tumorigenicity of a murine rhabdomyosarcoma model (75). We experimentally validated the *in vivo* tumorigenic impairment for HT1080 cells lacking SMG7, and our cell-based *in vitro* assays showed that the reduced migration and clonogenic capacities characteristic of the SMG7KO cells could be reproduced in the parental cells by inhibiting the SMG1 kinase, strongly suggesting that the impaired tumorigenicity might be attributed to NMD inhibition rather than to NMD-independent functions of the SMG7 protein (76). The necessity to perform our xenograft experiments in NOD scid gamma (NSG) mice, which is one of the most immunocompromised mouse strains, precludes us from assessing if the implanted SMG7KO cells can trigger a stronger immune response than that of parental or RESCUE cells. However, the IPA analysis conducted on the RNAseq dataset of the tumors revealed that the tumors formed by SMG7KO cells showed changes in gene expression that are consistent with increased inflammatory processes, results that agree with previous findings (77,78).

Our work uncovered a direct correlation between NMD activity and MMP9 expression levels, both *in vivo* and *in vitro*, and MMP9 expression has been associated with the malignant phenotype of many different cancer types (58,59,61–63,79–81). Consistently, we could show that the migration and anchorage-independent growth deficits in SMG7KO cells could be partially rescued by overexpressing recombinant MMP9. Considering the reported roles for MMP9 in the spreading of tumor cells, we hypothesize that NMD inhibited cells could show impaired metastatic capacity, and the use of experimental metastasis models (82) will be fundamental to understand if NMD inhibition could be used to limit the spreading of cancer cells to other organs. MMP9 expression has been shown to be modulated by epigenetic, transcriptional, and post-transcriptional mechanisms (83–88), and our preliminary experiments suggest that NMD inhibition results in diminished transcription of the MMP9 gene. However, the exact molecular mechanism remains to be elucidated. In addition, the forced overexpression of MMP9 in SMG7KO cells resulted only in a partial rescue of the anchorage-independent growth phenotype. We therefore envision that other de-regulated genes might also contribute to the observed phenotype. Our IPA analysis on tumor samples revealed many genes that could poten-

tially impact the tumorigenicity of HT1080 cells, including ICAM1 (89,90), ANGPTL2 (91) or LTF (92), and follow up studies are required to explore the potential contributions of these de-regulated genes.

Collectively, our results provide insights into the molecular mechanisms by which NMD activity benefits tumorigenicity of a classical cancer model system. Together with recent reports providing evidence for NMD's beneficial role in the development of a variety of different cancer types (22–25), our findings suggest that in many cases, inhibition of NMD might represent a promising strategy to reduce tumor growth and prevent metastasis.

DATA AVAILABILITY

All primary data is available upon request from the corresponding author. Illumina sequencing data has been deposited at GEO (https://www.ncbi.nlm.nih.gov/geo/) under accession numbers GSE232333 (HT1080 cell lines), and GSE232185 (tumor samples). The SILAC-MS data has been deposited in the PRIDE repository (http://www.ebi.ac.uk/pride) under the accession number PXD041853.

SUPPLEMENTARY DATA

Supplementary Data are available at NAR Cancer Online.

REFERENCES

1. Mühlemann,O. and Jensen,T.H. (2012) MRNP quality control goes regulatory. *Trends Genet.*, **28**, 70–77.
2. Doma,M.K. and Parker,R. (2007) RNA quality control in eukaryotes. *Cell*, **131**, 660–668.
3. Maquat,L.E., Kinniburgh,A.J., Rachmilewitz,E.A. and Ross,J. (1981) Unstable beta-globin mRNA in mRNA-deficient beta° thalassemia. *Cell*, **27**, 543–553.
4. Losson,R. and Lacroute,F. (1979) Interference of nonsense mutations with eukaryotic messenger RNA stability. *Proc. Natl. Acad. Sci. U.S.A.*, **76**, 5134–5137.
5. Peltz,S.W., Brown,A.H. and Jacobson,A. (1993) mRNA destabilization triggered by premature translational termination depends on at least three cis-acting sequence elements and one trans-acting factor. *Genes Dev.*, **7**, 1737–1754.

6. Mendell,J.T., Sharifi,N.A., Meyers,J.L., Martinez-Murillo,F. and Dietz,H.C. (2004) Nonsense surveillance regulates expression of diverse classes of mammalian transcripts and mutes genomic noise. *Nat. Genet.*, **36**, 1073–1078.

7. Tani,H., Imamachi,N., Salam,K.A., Mizutani,R., Ijiri,K., Irie,T., Yada,T., Suzuki,Y. and Akimitsu,N. (2012) Identification of hundreds of novel UPF1 target transcripts by direct determination of whole transcriptome stability. *RNA Biol.*, **9**, 1370–1379.

8. Wittmann,J., Hol,E.M. and Jäck,H.-M. (2006) hUPF2 Silencing identifies physiologic substrates of mammalian nonsense-mediated mRNA decay. *Mol. Cell. Biol.*, **26**, 1272–1287.

9. Yepiskoposyan,H., Aeschimann,F., Nilsson,D., Okoniewski,M. and Mühlemann,O. (2011) Autoregulation of the nonsense-mediated mRNA decay pathway in human cells. *RNA*, **17**, 2108–2118.

10. Colombo,M., Karousis,E.D., Bourquin,J., Bruggmann,R. and Mühlemann,O. (2017) Transcriptome-wide identification of NMD-targeted human mRNAs reveals extensive redundancy between SMG6- and SMG7-mediated degradation pathways. *RNA*, **23**, 189–201.

11. Karousis,E.D., Gypas,F., Zavolan,M. and Mühlemann,O. (2021) Nanopore sequencing reveals endogenous NMD-targeted isoforms in human cells. *Genome Biol.*, **22**, 223.

12. Boehm,V., Kueckelmann,S., Gerbracht,J.V., Kallabis,S., Britto-Borges,T., Altmüller,J., Krüger,M., Dieterich,C. and Gehring,N.H. (2021) SMG5-SMG7 authorize nonsense-mediated mRNA decay by enabling SMG6 endonucleolytic activity. *Nat. Commun.*, **12**, 3965.

13. Karousis,E.D. and Mühlemann,O. (2022) The broader sense of nonsense. *Trends Biochem. Sci.*, **47**, 921–935.

14. Zünd,D., Gruber,A.R., Zavolan,M. and Mühlemann,O. (2013) Translation-dependent displacement of UPF1 from coding sequences causes its enrichment in 3' UTRs. *Nat. Struct. Mol. Biol.*, **20**, 936–943.

15. Eberle,A.B., Lykke-Andersen,S., Mühlemann,O. and Jensen,T.H. (2009) SMG6 promotes endonucleolytic cleavage of nonsense mRNA in human cells. *Nat. Struct. Mol. Biol.*, **16**, 49–55.

16. Loh,B., Jonas,S. and Izaurralde,E. (2013) The SMG5-SMG7 heterodimer directly recruits the CCR4-NOT deadenylase complex to mRNAs containing nonsense codons via interaction with POP2. *Genes Dev.*, **27**, 2125–2138.

17. Huth,M., Santini,L., Galimberti,E., Ramesmayer,J., Titz-Teixeira,F., Sehlke,R., Oberhuemer,M., Stummer,S., Herzog,V., Garmhausen,M. *et al.* (2022) NMD is required for timely cell fate transitions by fine-tuning gene expression and regulating translation. *Genes Dev.*, **36**, 348–367.

18. Huang,L., Lou,C.H., Chan,W., Shum,E.Y., Shao,A., Stone,E., Karam,R., Song,H.W. and Wilkinson,M.F. (2011) RNA homeostasis governed by cell type-specific and branched feedback loops acting on NMD. *Mol. Cell*, **43**, 950–961.

19. Nasif,S., Contu,L. and Mühlemann,O. (2018) Beyond quality control: the role of nonsense-mediated mRNA decay (NMD) in regulating gene expression. *Semin. Cell Dev. Biol.*, **75**, 78–87.

20. Miller,J.N. and Pearce,D.a. (2014) Nonsense-mediated decay in genetic disease: friend or foe? *Mut. Res./Rev. Mut. Res.*, **762**, 52–64.

21. Tan,K., Stupack,D.G. and Wilkinson,M.F. (2022) Nonsense-mediated RNA decay: an emerging modulator of malignancy. *Nat. Rev. Cancer*, **22**, 437–451.

22. Zhang,Y., Xie,X., Yeganeh,P.N., Lee,D.-J., Valle-Garcia,D., Meza-Sosa,K.F., Junqueira,C., Su,J., Luo,H.R., Hide,W. *et al.* (2021) Immunotherapy for breast cancer using EpCAM aptamer tumor-targeted gene knockdown. *Proc. Natl. Acad. Sci. U.S.A.*, **118**, e2022830118.

23. Pastor,F., Kolonias,D., Giangrande,P.H. and Gilboa,E. (2010) Induction of tumour immunity by targeted inhibition of nonsense-mediated mRNA decay. *Nature*, **465**, 227–230.

24. Meraviglia-Crivelli,D., Villanueva,H., Zheleva,A., Villalba-Esparza,M., Moreno,B., Menon,A.P., Calvo,A., Cebollero,J., Barainka,M., de los Mozos,I.R. *et al.* (2022) IL-6/STAT3 signaling in tumor cells restricts the expression of frameshift-derived neoantigens by SMG1 induction. *Mol. Cancer*, **21**, 211.

25. Meraviglia-Crivelli,D., Villanueva,H., Menon,A.P., Zheleva,A., Moreno,B., Villalba-Esparza,M. and Pastor,F. (2022) A pan-tumor-siRNA aptamer chimera to block nonsense-mediated mRNA decay inflames and suppresses tumor progression. *Mol. Ther. Nucleic Acids*, **29**, 413–425.

26. Becker,J.P., Helm,D., Rettel,M., Stein,F., Hernandez-Sanchez,A., Urban,K., Gebert,J., Kloor,M., Neu-Yilik,G., von Knebel Doeberitz,M. *et al.* (2021) NMD inhibition by 5-azacytidine augments presentation of immunogenic frameshift-derived neoepitopes. *iScience*, **24**, 102389.

27. Lindeboom,R.G.H., Vermeulen,M., Lehner,B. and Supek,F. (2019) The impact of nonsense-mediated mRNA decay on genetic disease, gene editing and cancer immunotherapy. *Nat. Genet.*, **51**, 1645–1651.

28. Litchfield,K., Reading,J.L., Lim,E.L., Xu,H., Liu,P., Al-Bakir,M., Wong,Y.N.S., Rowan,A., Funt,S.A., Merghoub,T. *et al.* (2020) Escape from nonsense-mediated decay associates with anti-tumor immunogenicity. *Nat. Commun.*, **11**, 3800.

29. Hu,Z., Yau,C. and Ahmed,A.A. (2017) A pan-cancer genome-wide analysis reveals tumour dependencies by induction of nonsense-mediated decay. *Nat. Commun.*, **8**, 15943.

30. Lindeboom,R.G.H., Supek,F. and Lehner,B. (2016) The rules and impact of nonsense-mediated mRNA decay in human cancers. *Nat. Genet.*, **48**, 1112–1118.

31. Zhao,B. and Pritchard,J.R. (2019) Evolution of the nonsense-mediated decay pathway is associated with decreased cytolytic immune infiltration. *PLoS Comput. Biol.*, **15**, e1007467.

32. Ivanov,I., Lo,K.C., Hawthorn,L., Cowell,J.K. and Ionov,Y. (2007) Identifying candidate colon cancer tumor suppressor genes using inhibition of nonsense-mediated mRNA decay in colon cancer cells. *Oncogene*, **26**, 2873–2884.

33. Anczuków,O., Ware,M.D., Buisson,M., Zetoune,A.B., Stoppa-Lyonnet,D., Sinilnikova,O.M. and Mazoyer,S. (2008) Does the nonsense-mediated mRNA decay mechanism prevent the synthesis of truncated BRCA1, CHK2, and p53 proteins? *Hum. Mutat.*, **29**, 65–73.

34. Karam,R., Carvalho,J., Bruno,I., Graziadio,C., Senz,J., Huntsman,D., Carneiro,F., Seruca,R., Wilkinson,M.F. and Oliveira,C. (2008) The NMD mRNA surveillance pathway downregulates aberrant E-cadherin transcripts in gastric cancer cells and in CDH1 mutation carriers. *Oncogene*, **27**, 4255–4260.

35. Perrin-Vidoz,L., Sinilnikova,O.M., Stoppa-Lyonnet,D., Lenoir,G.M. and Mazoyer,S. (2002) The nonsense-mediated mRNA decay pathway triggers degradation of most BRCA1 mRNAs bearing premature termination codons. *Hum. Mol. Genet.*, **11**, 2805–2814.

36. Li,L., Geng,Y., Feng,R., Zhu,Q., Miao,B., Cao,J. and Fei,S. (2017) The Human RNA surveillance factor UPF1 modulates gastric cancer progression by targeting long non-coding RNA MALAT1. *Cell. Physiol. Biochem.*, **42**, 2194–2206.

37. Chang,L., Li,C., Guo,T., Wang,H., Ma,W., Yuan,Y., Liu,Q., Ye,Q. and Liu,Z. (2016) The human RNA surveillance factor UPF1 regulates tumorigenesis by targeting Smad7 in hepatocellular carcinoma. *J. Exp. Clin. Cancer Res.*, **35**, 8.

38. Cao,L., Qi,L., Zhang,L., Song,W., Yu,Y., Xu,C., Li,L., Guo,Y., Yang,L., Liu,C. *et al.* (2017) Human nonsense-mediated RNA decay regulates EMT by targeting the TGF-ß signaling pathway in lung adenocarcinoma. *Cancer Lett.*, **403**, 246–259.

39. Lu,J., Plank,T.-D., Su,F., Shi,X., Liu,C., Ji,Y., Li,S., Huynh,A., Shi,C., Zhu,B. *et al.* (2016) The nonsense-mediated RNA decay pathway is disrupted in inflammatory myofibroblastic tumors. *J. Clin. Invest.*, **126**, 3058–3062.

40. Zhou,Y., Li,Y., Wang,N., Li,X., Zheng,J. and Ge,L. (2019) UPF1 inhibits the hepatocellular carcinoma progression by targeting long non-coding RNA UCA1. *Sci. Rep.*, **9**, 6652.

41. Wang,D., Zavadil,J., Martin,L., Parisi,F., Friedman,E., Levy,D., Harding,H., Ron,D. and Gardner,L.B. (2011) Inhibition of nonsense-mediated RNA decay by the tumor microenvironment promotes tumorigenesis. *Mol. Cell. Biol.*, **31**, 3670–3680.

42. Reber,S., Mechtersheimer,J., Nasif,S., Aguila Benitez,J., Colombo,M., Domanski,M., Jutzi,D., Hedlund,E. and Ruepp,M.-.D. (2018) CRISPR-trap: a clean approach for the generation of gene knockouts and gene replacements in human cells. *Mol. Biol. Cell*, **29**, 75–83.

43. Nicholson,P., Joncourt,R. and Mühlemann,O. (2012) Analysis of nonsense-mediated mRNA decay in mammalian cells. *Curr. Protoc. Cell Biol.*, **Chapter 27**, Unit27.4.

44. Flury,V., Restuccia,U., Bachi,A. and Mühlemann,O. (2014) Characterization of phosphorylation- and RNA-dependent UPF1

interactors by quantitative proteomics. *J. Proteome Res.*, **13**, 3038–3053.

45. Gunasekera,K., Wüthrich,D., Braga-Lagache,S., Heller,M. and Ochsenreiter,T. (2012) Proteome remodelling during development from blood to insect-form trypanosoma brucei quantified by SILAC and mass spectrometry. *BMC Genomics*, **13**, 556.

46. Cox,J. and Mann,M. (2008) MaxQuant enables high peptide identification rates, individualized p.p.b.-range mass accuracies and proteome-wide protein quantification. *Nat. Biotechnol.*, **26**, 1367–1372.

47. UniProt Consortium (2019) UniProt: a worldwide hub of protein knowledge. *Nucleic Acids Res.*, **47**, D506–D515.

48. Venables,W.N. and Ripley,B.D. (2002) In: *Modern Applied Statistics with S Fourth*. Springer, NY.

49. Smyth,G.K., Michaud,J. and Scott,H.S. (2005) Use of within-array replicate spots for assessing differential expression in microarray experiments. *Bioinformatics*, **21**, 2067–2075.

50. Kammers,K., Cole,R.N., Tiengwe,C. and Ruczinski,I. (2015) Detecting significant changes in protein abundance. *EuPA Open Proteom*, **7**, 11–19.

51. Benjamini,Y. and Hochberg,Y. (1995) Controlling the false discovery rate: a practical and powerful approach to multiple testing. *J. R. Stat. Soc. Series B Stat. Methodol.*, **57**, 289–300.

52. Rasheed,S., Nelson-Rees,W.A., Toth,E.M., Arnstein,P. and Gardner,M.B. (1974) Characterization of a newly derived human sarcoma cell line (HT-1080). *Cancer*, **33**, 1027–1033.

53. Schwartz,M.P., Rogers,R.E., Singh,S.P., Lee,J.Y., Loveland,S.G., Koepsel,J.T., Witze,E.S., Montanez-Sauri,S.I., Sung,K.E., Tokuda,E.Y. *et al.* (2013) A quantitative comparison of Human HT-1080 fibrosarcoma cells and primary Human dermal fibroblasts identifies a 3D migration mechanism with properties unique to the transformed phenotype. *PLoS One*, **8**, e81689.

54. Harisi,R., Kenessey,I., Olah,J.N., Timar,F., Babo,I., Pogany,G., Paku,S. and Jeney,A. (2009) Differential inhibition of single and cluster type tumor cell migration. *Anticancer Res.*, **29**, 2981–2985.

55. Cha,H.J., Bae,S.K., Lee,H.Y., Lee,O.H., Sato,H., Seiki,M., Park,B.C. and Kim,K.W. (1996) Anti-invasive activity of ursolic acid correlates with the reduced expression of matrix metalloproteinase-9 (MMP-9) in HT1080 human fibrosarcoma cells. *Cancer Res.*, **56**, 2281–2284.

56. Gopalsamy,A., Bennett,E.M., Shi,M., Zhang,W.G., Bard,J. and Yu,K. (2012) Identification of pyrimidine derivatives as hSMG-1 inhibitors. *Bioorg. Med. Chem. Lett.*, **22**, 6636–6641.

57. Langer,L.M., Bonneau,F., Gat,Y. and Conti,E. (2021) Cryo-EM reconstructions of inhibitor-bound SMG1 kinase reveal an autoinhibitory state dependent on SMG8. *eLife*, **10**, 72353.

58. Ballin,M., Gomez,D.E., Sinha,C.C. and Thorgeirsson,U.P. (1988) Ras oncogene mediated induction of a 92kDa metalloproteinase; strong correlation with the malignant phenotype. *Biochem. Biophys. Res. Commun.*, **154**, 832–838.

59. Bernhard,E.J., Grubert,S.B. and Muschel,R.J. (1994) Direct evidence linking expression of matrix metalloproteinase 9 (92-kDa gelatinase/collagenase) to the metastatic phenotype in transformed rat embryo cells. *Proc. Natl Acad. Sci.*, **91**, 4293–4297.

60. Kessenbrock,K., Plaks,V. and Werb,Z. (2010) Matrix metalloproteinases: regulators of the tumor microenvironment. *Cell*, **141**, 52–67.

61. Wen,J., Yin,P., Li,L., Kang,G., Ning,G., Cao,Y., Gao,F., Su,Y., Wu,Y. and Zhang,X. (2020) Knockdown of matrix metallopeptidase 9 inhibits metastasis of oral squamous cell carcinoma cells in a zebrafish xenograft model. *Biomed. Res. Int.*, **2020**, 4350783.

62. Dong,H., Diao,H., Zhao,Y., Xu,H., Pei,S., Gao,J., Wang,J., Hussain,T., Zhao,D., Zhou,X. *et al.* (2019) Overexpression of matrix metalloproteinase-9 in breast cancer cell lines remarkably increases the cell malignancy largely via activation of transforming growth factor beta/SMAD signalling. *Cell Prolif.*, **52**, e12633.

63. Aalinkeel,R., Nair,B.B., Reynolds,J.L., Sykes,D.E., Mahajan,S.D., Chadha,K.C. and Schwartz,S.A. (2011) Overexpression of MMP-9 contributes to invasiveness of prostate cancer cell line LNCaP. *Immunol. Invest.*, **40**, 447–464.

64. Hua,J. and Muschel,R.J. (1996) Inhibition of matrix metalloproteinase 9 expression by a ribozyme blocks metastasis in a rat sarcoma model system. *Cancer Res.*, **56**, 5279–5284.

65. Hao,S. and Baltimore,D. (2009) The stability of mRNA influences the temporal order of the induction of genes encoding inflammatory molecules. *Nat. Immunol.*, **10**, 281–288.

66. Karousis,E.D., Nasif,S. and Mühlemann,O. (2016) Nonsense-mediated mRNA decay: novel mechanistic insights and biological impact. *Wiley Interdiscip. Rev. RNA*, **7**, 661–682.

67. He,F. and Jacobson,A. (2015) Nonsense-mediated mRNA decay: degradation of defective transcripts is only part of the story. *Annu. Rev. Genet.*, **49**, 339–366.

68. Lykke-Andersen,S. and Jensen,T.H. (2015) Nonsense-mediated mRNA decay: an intricate machinery that shapes transcriptomes. *Nat. Rev. Mol. Cell Biol.*, **16**, 665–677.

69. Metze,S., Herzog,V.A., Ruepp,M.-D. and Mühlemann,O. (2013) Comparison of EJC-enhanced and EJC-independent NMD in human cells reveals two partially redundant degradation pathways. *RNA*, **19**, 1432–1448.

70. Lykke-Andersen,S., Chen,Y., Ardal,B.R., Lilje,B., Waage,J., Sandelin,A. and Jensen,T.H. (2014) Human nonsense-mediated RNA decay initiates widely by endonucleolysis and targets snoRNA host genes. *Genes Dev.*, **28**, 2498–2517.

71. Wallmeroth,D., Lackmann,J.-W., Kueckelmann,S., Altmüller,J., Dieterich,C., Boehm,V. and Gehring,N.H. (2022) Human UPF3A and UPF3B enable fault-tolerant activation of nonsense-mediated mRNA decay. *EMBO J.*, **41**, e109191.

72. Yi,Z., Arvola,R.M., Myers,S., Dilsavor,C.N., Abu Alhasan,R., Carter,B.N., Patton,R.D., Bundschuh,R. and Singh,G. (2022) Mammalian UPF3A and UPF3B can activate nonsense-mediated mRNA decay independently of their exon junction complex binding. *EMBO J.*, **41**, e109202.

73. Vogelstein,B., Papadopoulos,N., Velculescu,V.E., Zhou,S., Diaz,L.A. and Kinzler,K.W. (2013) Cancer genome landscapes. *Science*, **339**, 1546–1558.

74. Oka,M., Xu,L., Suzuki,T., Yoshikawa,T., Sakamoto,H., Uemura,H., Yoshizawa,A.C., Suzuki,Y., Nakatsura,T., Ishihama,Y. *et al.* (2021) Aberrant splicing isoforms detected by full-length transcriptome sequencing as transcripts of potential neoantigens in non-small cell lung cancer. *Genome Biol.*, **22**, 9.

75. Steiner,A.J., Zheng,Y. and Tang,Y. (2023) Characterization of a rhabdomyosarcoma reveals a critical role for SMG7 in cancer cell viability and tumor growth. *Sci. Rep.*, **13**, 10152.

76. Luo,H., Cowen,L., Yu,G., Jiang,W. and Tang,Y. (2016) SMG7 is a critical regulator of p53 stability and function in DNA damage stress response. *Cell Discov.*, **2**, 15042.

77. Roberts,T.L., Ho,U., Luff,J., Lee,C.S., Apte,S.H., MacDonald,K.P.A., Raggat,L.J., Pettit,A.R., Morrow,C.A., Waters,M.J. *et al.* (2013) Smg1 haploinsufficiency predisposes to tumor formation and inflammation. *Proc. Natl. Acad. Sci. U.S.A.*, **110**, E285–E294.

78. Johnson,J.L., Stoica,L., Liu,Y., Zhu,P.J., Bhattacharya,A., Buffington,S.A., Huq,R., Eissa,N.T., Larsson,O., Porse,B.T. *et al.* (2019) Inhibition of Upf2-dependent nonsense-mediated decay leads to behavioral and neurophysiological abnormalities by activating the immune response. *Neuron*, **104**, 665–679.

79. Hiratsuka,S., Nakamura,K., Iwai,S., Murakami,M., Itoh,T., Kijima,H., Shipley,J.M., Senior,R.M. and Shibuya,M. (2002) MMP9 induction by vascular endothelial growth factor receptor-1 is involved in lung-specific metastasis. *Cancer Cell*, **2**, 289–300.

80. Herr,M.J., Kotha,J., Hagedorn,N., Smith,B. and Jennings,L.K. (2013) Tetraspanin CD9 promotes the invasive phenotype of human fibrosarcoma cells via upregulation of matrix metalloproteinase-9. *PLoS One*, **8**, e67766.

81. Mehner,C., Hockla,A., Miller,E., Ran,S., Radisky,D.C. and Radisky,E.S. (2014) Tumor cell-produced matrix metalloproteinase 9 (MMP-9) drives malignant progression and metastasis of basal-like triple negative breast cancer. *OncoTargets Ther.*, **5**, 2736–2749.

82. Khanna,C. and Hunter,K. (2005) Modeling metastasis in vivo. *Carcinogenesis*, **26**, 513–523.

83. Ma,Z., Shah,R.C., Chang,M.J. and Benveniste,E.N. (2004) Coordination of cell signaling, chromatin remodeling, histone modifications, and regulator recruitment in Human matrix metalloproteinase 9 gene transcription. *Mol. Cell. Biol.*, **24**, 5496–5509.

84. Yan,C. and Boyd,D.D. (2007) Regulation of matrix metalloproteinase gene expression. *J. Cell. Physiol.*, **211**, 19–26.

85. Zhao,X. and Benveniste,E.N. (2008) Transcriptional activation of human matrix metalloproteinase-9 gene expression by multiple co-activators. *J. Mol. Biol.*, **383**, 945–956.

86. Takagi,S., Simizu,S. and Osada,H. (2009) Reck negatively regulates matrix metalloproteinase-9 transcription. *Cancer Res.*, **69**, 1502–1508.

87. Labrie,M. and St-Pierre,Y. (2013) Epigenetic regulation of mmp-9 gene expression. *Cell. Mol. Life Sci.*, **70**, 3109–3124.

88. Chenette,D.M., Cadwallader,A.B., Antwine,T.L., Larkin,L.C., Wang,J., Olwin,B.B. and Schneider,R.J. (2016) Targeted mRNA decay by RNA binding protein AUF1 regulates adult muscle stem cell fate, promoting skeletal muscle integrity. *Cell Rep.*, **16**, 1379–1390.

89. Song Gho,Y., Kim,P.N., Li,H.C., Elkin,M. and Kleinman,H.K. (2001) Stimulation of tumor growth by human soluble intercellular adhesion molecule-1. *Cancer Res.*, **61**, 4253–4257.

90. Rosette,C., Roth,R.B., Oeth,P., Braun,A., Kammerer,S., Ekblom,J. and Denissenko,M.F. (2005) Role of ICAM1 in invasion of human breast cancer cells. *Carcinogenesis*, **26**, 943–950.

91. Kadomatsu,T., Endo,M., Miyata,K. and Oike,Y. (2014) Diverse roles of ANGPTL2 in physiology and pathophysiology. *Trends Endocrinol. Metab.*, **25**, 245–254.

92. Wei,L., Zhang,X., Wang,J., Ye,Q., Zheng,X., Peng,Q., Zheng,Y., Liu,P., Zhang,X., Li,Z. *et al.* (2020) Lactoferrin deficiency induces a pro-metastatic tumor microenvironment through recruiting myeloid-derived suppressor cells in mice. *Oncogene*, **39**, 122–135.